A&A 430, 165–186 (2005)
DOI: 10.1051/0004-6361:20041272

Astronomy & Astrophysics

Local kinematics of K and M giants from CORAVEL/Hipparcos/Tycho-2 data⋆,⋆⋆

Revisiting the concept of superclusters

B. Famaey[1,⋆⋆⋆], A. Jorissen[1,†], X. Luri[2], M. Mayor[3], S. Udry[3], H. Dejonghe[4], and C. Turon[5]

[1] Institut d'Astronomie et d'Astrophysique, Université Libre de Bruxelles, CP 226, Boulevard du Triomphe, 1050 Bruxelles, Belgium
e-mail: [bfamaey;ajorisse]@astro.ulb.ac.be
[2] Departament d'Astronomia i Meteorologia, Universitat de Barcelona, Avda. Diagonal 647, 08028 Barcelona, Spain
[3] Observatoire de Genève, Chemin des Maillettes 51, 1290 Sauverny, Switzerland
[4] Sterrenkundig Observatorium, Universiteit Gent, Krijgslaan 281, 9000 Gent, Belgium
[5] Observatoire de Paris, section de Meudon, GEPI/CNRS UMR 8111, 92195 Meudon CEDEX, France

Received 11 May 2004 / Accepted 21 September 2004

Abstract. The availability of the Hipparcos Catalogue has triggered many kinematic and dynamical studies of the solar neighbourhood. Nevertheless, those studies generally lacked the third component of the space velocities, i.e., the radial velocities. This work presents the kinematic analysis of 5952 K and 739 M giants in the solar neighbourhood which includes for the first time radial velocity data from a large survey performed with the CORAVEL spectrovelocimeter. It also uses proper motions from the Tycho-2 catalogue, which are expected to be more accurate than the Hipparcos ones. An important by-product of this study is the observed fraction of only 5.7% of spectroscopic binaries among M giants as compared to 13.7% for K giants. After excluding the binaries for which no center-of-mass velocity could be estimated, 5311 K and 719 M giants remain in the final sample.

The UV-plane constructed from these data for the stars with precise parallaxes ($\sigma_\pi/\pi \leq 20\%$) reveals a rich small-scale structure, with several clumps corresponding to the Hercules stream, the Sirius moving group, and the Hyades and Pleiades superclusters. A maximum-likelihood method, based on a Bayesian approach, has been applied to the data, in order to make full use of all the available stars (not only those with precise parallaxes) and to derive the kinematic properties of these subgroups. Isochrones in the Hertzsprung-Russell diagram reveal a very wide range of ages for stars belonging to these groups. These groups are most probably related to the dynamical perturbation by transient spiral waves (as recently modelled by De Simone et al. 2004) rather than to cluster remnants. A possible explanation for the presence of young group/clusters in the same area of the UV-plane is that they have been put there by the spiral wave associated with their formation, while the kinematics of the older stars of our sample has also been disturbed by the same wave. The emerging picture is thus one of *dynamical streams* pervading the solar neighbourhood and travelling in the Galaxy with similar space velocities. The term *dynamical stream* is more appropriate than the traditional term *supercluster* since it involves stars of different ages, not born at the same place nor at the same time. The position of those streams in the UV-plane is responsible for the vertex deviation of $16.2° \pm 5.6°$ for the whole sample. Our study suggests that the vertex deviation for younger populations could have the same *dynamical* origin.

The underlying velocity ellipsoid, extracted by the maximum-likelihood method after removal of the streams, is not centered on the value commonly accepted for the radial antisolar motion: it is centered on $\langle U \rangle = -2.78 \pm 1.07$ km s^{-1}. However, the full data set (including the various streams) *does* yield the usual value for the radial solar motion, when properly accounting for the biases inherent to this kind of analysis (namely, $\langle U \rangle = -10.25 \pm 0.15$ km s^{-1}). This discrepancy clearly raises the essential question of how to derive the solar motion in the presence of dynamical perturbations altering the kinematics of the solar neighbourhood: does there exist in the solar neighbourhood a subset of stars having no net radial motion which can be used as a reference against which to measure the solar motion?

Key words. Galaxy: kinematics and dynamics – Galaxy: disk – Galaxy: solar neighbourhood – Galaxy: evolution – Galaxy: structure – stars: kinematics

⋆ Based on observations performed at the Swiss 1m-telescope at OHP, France, and on data from the ESA Hipparcos astrometry satellite.

⋆⋆ Full Table A.1 is only available in electronic form at the CDS via anonymous ftp to cdsarc.u-strasbg.fr (130.79.128.5) or via http://cdsweb.u-strasbg.fr/cgi-bin/qcat?J/A+A/430/165

⋆⋆⋆ Research Assistant, FRIA.

† Senior Research Associate, FNRS.

1. Introduction

The kinematics of stars in the solar neighbourhood, studied from proper motions and radial velocities, has long been acknowledged to be an essential element for the understanding of the structure and evolution of the Galaxy as a whole (e.g. Schwarzschild 1907; Lindblad 1925; Oort 1927). The story of the efforts to obtain the necessary data is standard textbook fare, and nicely illustrates how theoretical progress and data acquisition have to go hand in hand if one wants to gain insight into the true nature of our Galaxy. Clearly, another chapter in this story has begun with the Hipparcos satellite mission (ESA 1997), that provided accurate parallaxes and proper motions for a large number of stars (about 118 000): with accurate parallaxes available, it was no longer necessary to resort to photometric distances. The Hipparcos data enabled several kinematic studies of the solar neighbourhood, but those studies generally lacked radial velocity data. A first glimpse of how Hipparcos data could improve our knowledge of stellar motions in the Galaxy was given by Kovalevsky (1998); then, Dehnen & Binney (1998) used Hipparcos proper motions to derive some fundamental kinematic parameters of the solar neighbourhood. They did not use radial velocities from the literature because, at that time, radial velocities had been measured preferentially for high proper motions stars and their use would have introduced a kinematic bias. Hipparcos data were also used by Chereul et al. (1998) to derive the small scale structure of the velocity distribution of early-type stars in the solar neighbourhood.

The situation has dramatically improved thanks to the efforts of a large European consortium to obtain radial velocities of Hipparcos stars later than about F5 (Udry et al. 1997). The sample includes Hipparcos "survey" stars (flag S in field H68 of the Hipparcos Catalogue), and stars from other specific programmes. This unique database, comprising about 45 000 stars measured with the CORAVEL spectrovelocimeter (Baranne et al. 1979) at a typical accuracy of 0.3 km s^{-1}, combines high precision and the absence of kinematic bias. It thus represents an unprecedented data set to test the results obtained by previous kinematic studies based solely on Hipparcos data. Another feature of the present study is the use of Tycho-2 proper motions, which combine Hipparcos positions with positions from much older catalogues (Høg et al. 2000). They represent a subsantial improvement over the Hipparcos proper motions themselves, which are based on very accurate positions, but extending over a limited 3-year time span. Results from the Geneva-Copenhagen survey for about 14 000 F and G dwarfs present in the CORAVEL database have been recently published by Nordström et al. (2004). The present paper, on the other hand, concentrates on the K and M giants from the CORAVEL database.

According to the classical theory of moving groups, early-type stars are not good probes to determine global characteristics of the Galaxy because these stars are young and still carry the kinematic signature of their place of birth. As a consequence, their distribution in velocity space is clumpy (e.g. de Bruijne et al. 1997; Figueras et al. 1997; de Zeeuw et al. 1999). These inhomogeneities can be spatially confined groups of young stars (OB associations in the Gould's belt, young clusters) but can also be spatially extended groups. There is, however, some confusion in the literature about the related terminology. Eggen (1994) defines a "supercluster" as a group of stars gravitationally unbound that share the same kinematics and may occupy extended regions in the Galaxy, and a "moving group" as the part of the supercluster that enters the solar neighbourhood and can be observed all over the sky. Unfortunately, the same term "moving group" is sometimes also applied to OB associations (e.g. de Zeeuw et al. 1999). It has long been known that, in the solar vicinity, there are several superclusters and moving groups that share the same space motions as well-known open clusters (Eggen 1958). The best documented groups (see Montes et al. 2001, and references therein) are the Hyades supercluster associated with the Hyades cluster (600 Myr) and the Ursa Major group (also known as the Sirius supercluster) associated with the UMa cluster of stars (300 Myr). Another kinematic group called the Local Association or Pleiades moving group is a reasonably coherent kinematic group with embedded young clusters and associations like the Pleiades, α Persei, NGC 2516, IC 2602 and Scorpius-Centaurus, with ages ranging from about 20 to 150 Myr. Two other young moving groups are the IC 2391 supercluster (35−55 Myr) and the Castor moving group (200 Myr). The kinematic properties of all these moving groups and superclusters are listed by Montes et al. (2001) and Chereul et al. (1999). However, the recent observation (e.g. Chereul et al. 1998, 1999) that some of those superclusters involve early-type stars spanning a wide range of ages contradicts the classical hypothesis that supercluster stars share a common origin: Chereul et al. (1998) propose that the supercluster-like velocity structure is just a chance juxtaposition of several cluster remnants.

Nevertheless, significant clumpiness in velocity space has also been recently reported for *late-type* stars (Dehnen 1998), thus raising the questions of the age of those late-type stars and of the exact origin of this clumpiness. For example, Montes et al. (2001) suppose that, if a late-type star belongs to a moving group or supercluster, it may be considered as a sign that the star is young, an assumption that will be largely challenged by the results of this paper. Here, we attack the problem from another point of view by restricting our study of stellar kinematics to late-type giants (of spectral types K and M), without any a priori hypothesis on their motion or age.

The present paper is organized as follows. Section 2 describes the various data sets used in the present study. The kinematic analysis of the data and its implications for the dynamics of our Galaxy are presented in Sect. 3. The summary and conclusions are given in Sect. 4.

2. The data

2.1. Selection criteria

Our stellar sample is the intersection of several data sets: (i) in a first step, all stars with spectral types K and M appearing in field H76 of the Hipparcos Catalogue (ESA 1997) have been selected, and the Hipparcos parallaxes have been used in the present study; (ii) Proper motions were taken from the

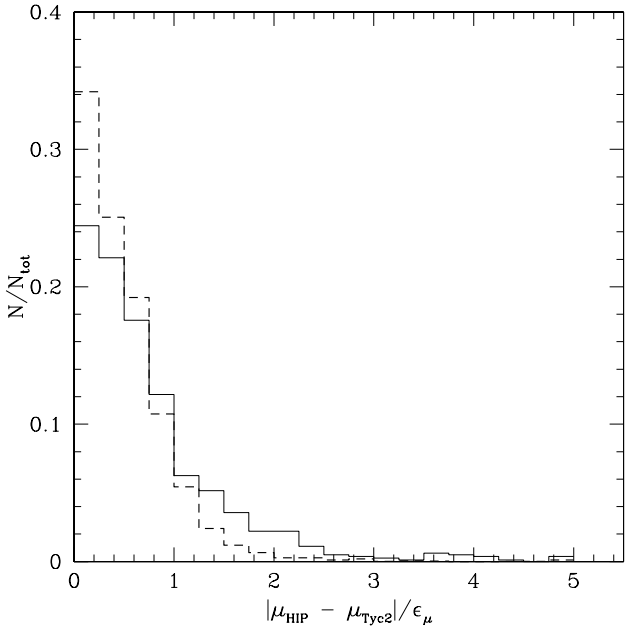

Fig. 1. Difference between the Hipparcos and Tycho-2 proper-motion moduli, normalized by the root mean square of the standard errors on the Hipparcos and Tycho-2 proper motions, denoted ϵ_μ. The solid line refers to the 859 spectroscopic binaries (SB) present in our sample, whereas the dashed line corresponds to the 5832 non-SB stars. Note that the sample of binaries contains more cases where the Hipparcos and Tycho-2 proper motions differ significantly, in agreement with the argument of Kaplan & Makarov (2003).

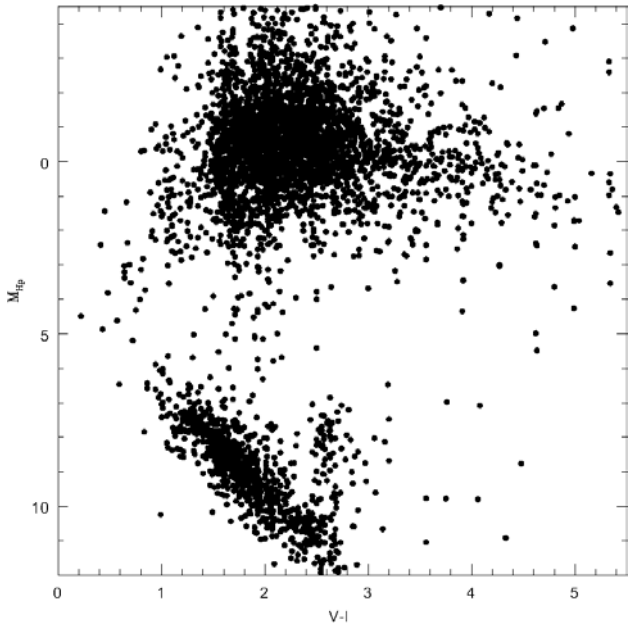

Fig. 2. Crude Hertzsprung-Russell diagram for the Hipparcos M stars with positive parallaxes.

Tycho-2 catalogue (Høg et al. 2000). These proper motions are more accurate than the Hipparcos ones. Figure 1 compares the proper motions from Tycho-2 and Hipparcos, and reveals that the Tycho-2 proper motions are sufficiently different from the Hipparcos ones (especially for binaries) to warrant the use of the former in the present study; (iii) Radial-velocity data for stars belonging to this first list (stars with spectral type K and M) have then been retrieved from the CORAVEL database. Only stars from the northern hemisphere ($\delta > 0°$), observed with the 1-m Swiss telescope at the *Haute-Provence Observatory*, have been considered. As described by Udry et al. (1997), all stars from the Hipparcos survey (including all stars brighter than $V = 7.3 + 1.1|\sin b|$ for spectral types later than G5, where b is the galactic latitude; those stars are flagged "S" in field H68 of the Hipparcos Catalogue) are present in the CORAVEL database. Besides the survey, stars from several other Hipparcos programmes, dealing with galactic studies and requiring radial velocities, were also monitored with CORAVEL. The CORAVEL database finally contains stars monitored for other purposes (e.g., binarity or rotation), but they represent a small fraction of the Hipparcos survey stars.

The sample resulting from the intersection of these 3 data sets was further cleaned as follows. First, a crude Hertzsprung-Russell diagram for all the M-type stars of the Hipparcos Catalogue has been constructed from distances estimated from a simple inversion of the parallax (Fig. 2), and reveals a clear separation between dwarfs and giants. Clearly, all M stars with $M_{Hp} < 4$ must be giants. For K-type stars with a relative parallax error less than 20%, the Hertzsprung-Russell diagram (Fig. 3) shows that the giant branch connects to the main sequence around $(V - I = 0.75, M_{Hp} = 4)$. Therefore, in order to select only K and M giants, only stars with $M_{Hp} < 4$ were kept in the sample. For K stars, the stars with $V - I < 0.75$ and $M_{Hp} > 2$ were eliminated to avoid contamination by K dwarfs. Diagnostics based on the radial-velocity variability and on the CORAVEL cross-correlation profiles, combined with literature searches, allowed us to further screen out stars with peculiar spectra, such as T Tau stars, Mira variables and S stars. T Tau stars have been eliminated because they belong to a specific young population; S stars because they are a mixture of extrinsic and intrinsic stars, which have different population characteristics (Van Eck & Jorissen 2000); Mira variables because their center-of-mass radial velocity is difficult to derive from the optical spectrum, where confusion is introduced by the pulsation (Alvarez et al. 2001).

The primary sample includes 5952 K giants and 739 M giants (6691 stars). 86% of those stars are "survey" stars: our sample is thus complete for the K and M giants brighter than $V = 7.3 + 1.1|\sin b|$. Thus, for a typical giant star with $M_V = 0$, this magnitude threshold translates into distances of 290 pc in the galactic plane and 480 pc in the direction of the galactic pole (these values are, however, very sensitive to the adopted absolute magnitude, and become 45 pc for a subgiant star with $M_V = +4$ in the galactic plane, and 2900 pc for a supergiant star with $M_V = -5$, corresponding to the range of luminosities present in our sample; see Sect. 3.3.6). The final step in the preparation and cleaning of the sample involves the identification of the spectroscopic binaries, as described in Sect. 2.2.

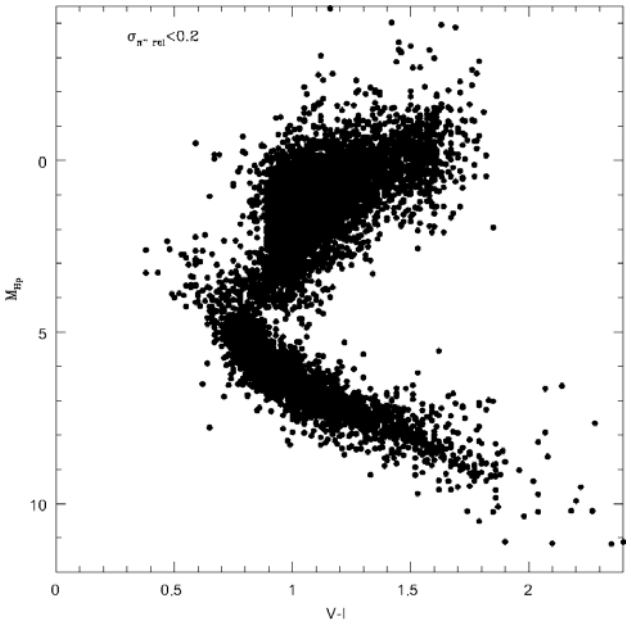

Fig. 3. Crude Hertzsprung-Russell diagram for the Hipparcos K stars with a relative error on the parallax less than 20%.

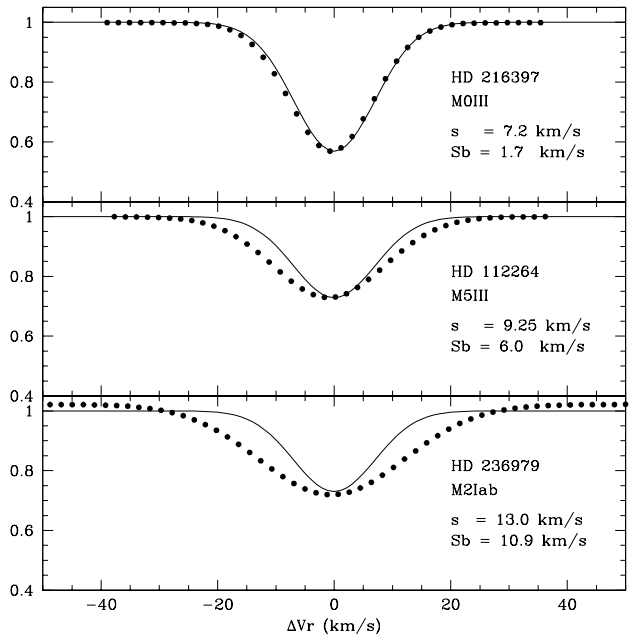

Fig. 4. The concept of line-width parameter $Sb = (s^2 - s_0^2)^{1/2}$ is illustrated here by comparing the CORAVEL cross-correlation (smoothed) profiles (black dots) of 3 M giants or supergiants with the Gaussian instrumental profile (of sigma s_0 = 7 km s^{-1}; solid line). Each profile corresponds to a single radial-velocity measurement for the given stars. The s value listed in the above panels refers to the sigma parameter of a Gaussian fitted to the observed correlation profile.

2.2. Binaries

The identification of the binaries, especially those with large velocity amplitudes, is an important step in the selection process, because kinematic studies should make use of the center-of-mass velocity. In order to identify those, the observing strategy was to obtain at least two radial-velocity measurements per star, spanning 2 to 3 yr. Monte-Carlo simulations reveal that, with such a strategy, binaries are detected with an efficiency better than 50 percent (Udry et al. 1997).

Since late-type giants exhibit intrinsic radial velocity jitter (Van Eck & Jorissen 2000), the identification of binaries requires a specific strategy, which makes use of the $(Sb, \sigma_0(v_{r0}))$ diagram (Fig. 5), where v_{r0} is the measured radial velocity. The parameter Sb is a measure of the intrinsic width of the cross-correlation profile, i.e., corrected from the instrumental width (see Fig. 4 for more precise definitions). The CORAVEL instrumental profile is obtained from the observation of the cross-correlation dip of minor planets reflecting the sun light, after correction for the solar rotational velocity and photospheric turbulence (see Benz & Mayor 1981 for more details). The Sb parameter is directly related to the average spectral line width, which is in turn a function of spectral type and luminosity, the later-type and more luminous stars having larger Sb values. On the other hand, the measurement error $\bar{\epsilon}$ has been quadratically subtracted from the radial velocity standard deviation $\sigma(v_{r0})$ to yield the effective standard deviation $\sigma_0(v_{r0})$.

The identification of binaries among K or M giants involves different steps. The standard χ^2 variability test, comparing the standard deviation $\sigma(v_{r0})$ of the measurements to their uncertainty $\bar{\epsilon}$, cannot be applied to M giants, because intrinsic radial-velocity variations ("jitter") associated with envelope pulsations would flag them as velocity variables in almost all cases. Therefore, in a first step, M giants having $\sigma_0(v_{r0}) \geq 1$ km s^{-1} have been monitored with the ELODIE spectrograph (Baranne et al. 1996) at the *Haute-Provence Observatory* (France) since August 2000 (Jorissen et al. 2004). These supplementary data points made it possible to distinguish orbital variations from radial-velocity jitter by a simple visual inspection of the data. It turns out that, in the $(Sb, \sigma_0(v_{r0}))$ diagram, all the confirmed binaries (filled symbols in the lower panel of Fig. 5) are located in the upper left corner, and are clearly separated from the bulk of the sample. Stars located below the dashed line in Fig. 5 may be supposed to be single (although some very long-period binaries, with $P \gtrsim 10$ y, may still hide among those). Their radial velocity dispersion suffers from a jitter which clearly increases with increasing spectral line-width, as represented by the parameter Sb. For very large values of Sb (in excess of about 9 km s^{-1}), the diagram is populated almost exclusively by supergiants (star symbols in the lower panel of Fig. 5). Many semi-regular and irregular variables are located in the intermediate region, with $5 \lesssim Sb \lesssim 9$ km s^{-1}. Strangely enough, spectroscopic binaries seem to be lacking in this region. A more detailed discussion of the properties of the binaries found among M giants is deferred to a forthcoming paper (see Jorissen et al. 2004, for a preliminary account).

For K giants, no such structure is apparent in the $(Sb, \sigma_0(v_{r0}))$ diagram. It has been checked that the distribution of stars along a $(N-1)[\sigma(v_{r0})/\epsilon]^2$ axis (where N is the number of measurements for a given star) follows a χ^2 distribution, as expected (e.g., Jorissen & Mayor 1988). This holds true irrespective of the Sb value, thus confirming the absence of structure in the $(Sb, \sigma_0(v_{r0}))$ diagram. The binaries among K giants may thus be identified by a straight χ^2 test. A 1% threshold for

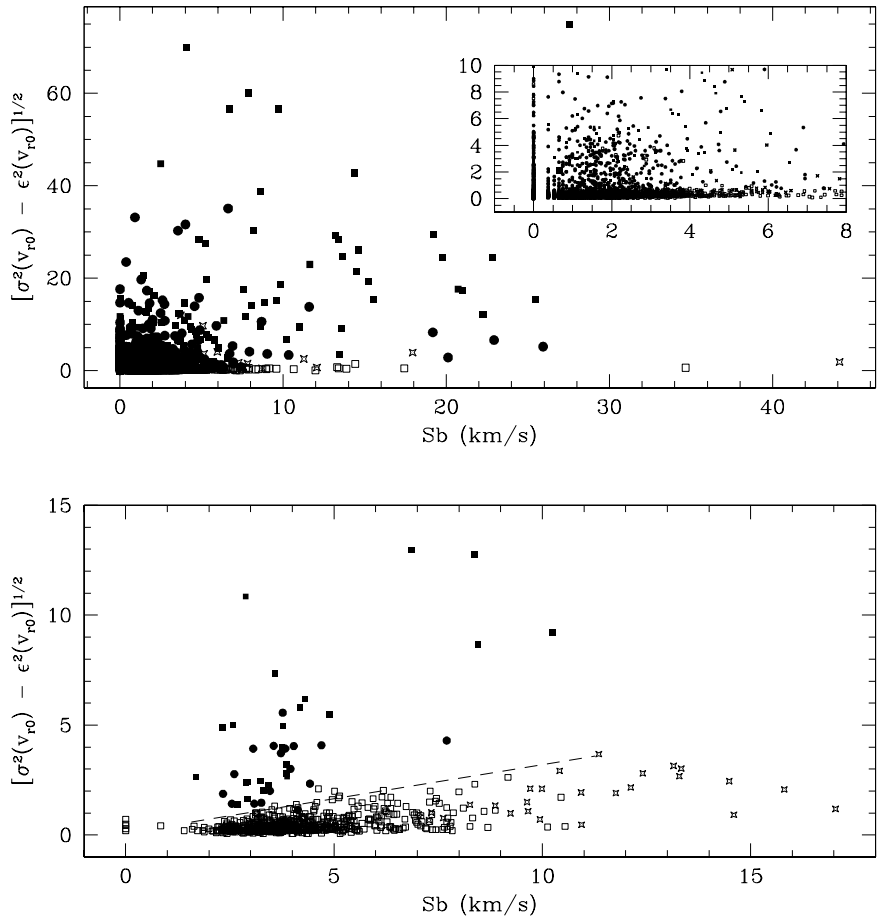

Fig. 5. The $(Sb, \sigma_0(v_{r0}))$ diagram (see text) for K (*upper panel*, and zoom inside) and M giants (*lower panel*). Star symbols denote supergiant stars, filled symbols denote spectroscopic binaries with (squares) or without (circles) center-of-mass velocity available.

the first kind risk (of rejecting the null hypothesis that the star is not a binary while this is actually true, i.e., of considering the star as binary while it is actually single) has been chosen in the present study.

Among M giants, 42 binaries are found (corresponding to an *observed* frequency of spectroscopic binaries of 42/739, or 5.7%). Among the 5952 K giants, 817 spectroscopic binaries are found, corresponding to a frequency of 13.7%. The large difference between these two frequencies hints at some underlying physical cause, to be discussed in a forthcoming paper (see Jorissen et al. 2004, for a preliminary discussion). Most of the spectroscopic binaries (SBs) detected among our samples of K and M giants are first detections. This large list of new SBs constitutes an important by-product of the present work. The new binaries are identified in Table A.1 (flags 0, 1, 5, 6 and 9 in Col. 24 of Table A.1) and will be the topic of a separate paper.

Among this total sample of 859 spectroscopic binaries, the center-of-mass velocity could be computed (whenever the available measurements were numerous enough to derive an orbit), estimated (in the case of low-amplitude orbits) or taken from the literature for 216 systems only, thus leaving 643 binaries which had to be discarded from the kinematic study, because no reliable center-of-mass velocity could be estimated.

After excluding those large-amplitude binaries as well as the dubious cases, 5311 K giants and 719 M giants remain in the final sample. Figure 6 shows the distribution of our final sample on the sky. Among this final sample of 6030 stars, 5397 belong to the Hipparcos "survey".

3. Kinematic analysis

In this section, we present the kinematic analysis of the data. Although the velocity distribution is a function of position in the Galaxy, it will be assumed here that our *local* stellar sample may be used to derive the properties of the velocity distribution at the location of the Sun if we correct the data for the effects of differential galactic rotation. First, we analyze the kinematics of the sample restricted to the 2774 stars with parallaxes accurate to better than 20%. In a second approach, designed to make full use of the 6030 available stars but without being affected by the biases appearing when dealing with low-precision parallaxes, the kinematic parameters are evaluated with a Monte-Carlo method. Although easy to implement, the Monte Carlo method faces some limitations (the parallaxes were drawn from a Gaussian distribution centered on the *observed* parallax, not the true one as it should be). Therefore, in a third approach, we make use of a Bayesian method (the LM method; Luri et al. 1996), which allows us to derive

simultaneously maximum likelihood estimators of luminosity and kinematic parameters, and which can identify possible groups present in the sample by performing a cluster analysis.

In all cases, we correct for differential Galactic rotation in order to deal with the true velocity of a star relative to the Local Standard of Rest (the LSR is a reference frame in circular orbit in the Galactic plane at the galactocentric distance of the Sun). Given the observed values of the radial velocity v_{r0} and the proper motions μ_{l0} and μ_{b0}, the corrected values are (Trumpler & Weaver 1953):

$$v_r = v_{r0} - A\,d\cos^2 b \sin 2l \tag{1}$$

$$\kappa\mu_l = \kappa\mu_{l0} - A\cos 2l - B \tag{2}$$

$$\kappa\mu_b = \kappa\mu_{b0} + 1/2\,A \sin 2b \sin 2l, \tag{3}$$

where κ is the factor to convert proper motions into space velocities, and d is the distance to the Sun. We used the values of the Oort constants A and B derived by Feast & Whitelock (1997) from Hipparcos Cepheids, i.e. $A = 14.82\,\mathrm{km\,s^{-1}\,kpc^{-1}}$ and $B = -12.37\,\mathrm{km\,s^{-1}\,kpc^{-1}}$. The observed velocity is, after that correction, a combination of the peculiar velocity of the star and that of the Sun relative to the LSR.

3.1. Analysis of the sample restricted to stars with the most precise parallaxes

The components of the velocity of a star with respect to the Sun in the Cartesian coordinate system associated with galactic coordinates are the velocity towards the galactic center U, the velocity in the direction of Galactic rotation V, and the vertical velocity W. The basic technique to calculate U, V and W is to invert the parallax to estimate the distance and then use the proper motions and radial velocities as given by Eqs. (1)–(3). This simple procedure faces two major difficulties: (i) the inverse parallax is a biased estimator of the distance (especially when the relative error on the parallax is high); and (ii) the individual errors on the velocities cannot be derived from a simple first-order linear propagation of the individual errors on the parallaxes. It is thus extremely hard to estimate an error on the average velocities. If we limit the sample to the stars with a relative parallax error smaller than 10%, we are left with 786 stars, which is too small a sample to analyze the general behaviour of the K and M giants in the solar neighbourhood. We choose instead to restrict the sample to the stars with a relative parallax error smaller than 20%, in such a way that 2774 stars (2524 K and 250 M) remain. In that case the classical first order approximation for the calculation of the errors may still be applied (and the bias is very small, see Brown et al. 1997), which yields from the errors on the proper motions, radial velocities and parallaxes

$$\begin{aligned}\langle\epsilon_U\rangle &= 4.03\,\mathrm{km\,s^{-1}}\\ \langle\epsilon_V\rangle &= 3.22\,\mathrm{km\,s^{-1}}\\ \langle\epsilon_W\rangle &= 2.54\,\mathrm{km\,s^{-1}}.\end{aligned} \tag{4}$$

The contribution of the measurement errors to the uncertainty on the sample mean velocity is $N^{-1/2}$ times the values given by (4), where N(=2774) is the sample size. This contribution is in fact negligible with respect to the "Poisson noise" (obtained from the intrinsic velocity dispersion of the sample, see Eq. (8)). For the stars with a relative parallax error smaller than 20%, we obtain

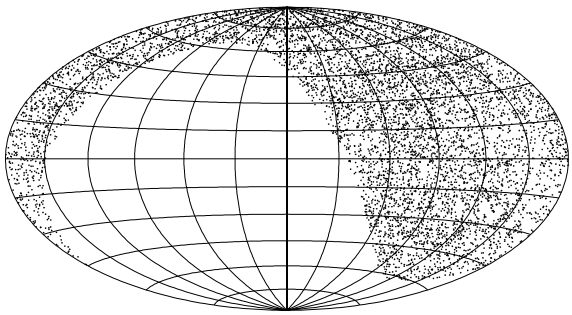

Fig. 6. Distribution of the final sample on the sky, in galactic coordinates, the galactic center being at the center of the map. The selection criterion $\delta > 0°$ is clearly apparent on this map.

$$\begin{aligned}\langle U\rangle &= -10.24 \pm 0.66\,\mathrm{km\,s^{-1}}\\ \langle V\rangle &= -20.51 \pm 0.43\,\mathrm{km\,s^{-1}}\\ \langle W\rangle &= -7.77 \pm 0.34\,\mathrm{km\,s^{-1}}.\end{aligned} \tag{5}$$

If there is no net radial and vertical motion at the solar position in the Galaxy, we have hence estimated $U_\odot = -\langle U\rangle$ and $W_\odot = -\langle W\rangle$ (see however Sect. 3.3.6).

Knowing that $\langle V\rangle$ is affected by the asymmetric drift, which implies that the larger a stellar sample's velocity dispersion is, the more it lags behind the circular Galactic rotation, it is interesting to compare the mean value of V for the K and M giants separately. For the 250 M giants, we obtain

$$\langle V\rangle = -23.42 \pm 1.48\,\mathrm{km\,s^{-1}} \tag{6}$$

while for the 2524 K giants we obtain

$$\langle V\rangle = -20.22 \pm 0.44\,\mathrm{km\,s^{-1}}. \tag{7}$$

This difference (at the 2σ level) between the two subsamples can be understood in terms of the age-velocity dispersion relation. Indeed, the M giants must be a little older than the K giants on average because only the low-mass stars can reach the spectral type M on the Red Giant Branch and because the lifetime on the main sequence is longer for lower mass stars. This implies that the subsample of M giants has a larger velocity dispersion and rotates more slowly about the Galactic Center than the subsample of K giants, in agreement with the asymmetric drift relation.

The velocity dispersion tensor is defined as $\langle(\mathbf{v} - \langle\mathbf{v}\rangle) \otimes (\mathbf{v} - \langle\mathbf{v}\rangle)\rangle$. The diagonal components are the square of the velocity dispersions while the mixed components correspond to the covariances. For the stars with a relative parallax error smaller than 20%, we obtain the classical ordering for the diagonal components, i.e. $\sigma_U > \sigma_V > \sigma_W$:

$$\begin{aligned}\sigma_U &= 34.46 \pm 0.46\,\mathrm{km\,s^{-1}}\\ \sigma_V &= 22.54 \pm 0.30\,\mathrm{km\,s^{-1}}\\ \sigma_W &= 17.96 \pm 0.24\,\mathrm{km\,s^{-1}}.\end{aligned} \tag{8}$$

The asymmetric drift relation predicts a linear dependence of $\langle v \rangle = \langle V \rangle + V_\odot$ with the radial velocity dispersion σ_U^2. If we adopt the peculiar velocity of the Sun from Dehnen & Binney (1998), $V_\odot = 5.25\,\mathrm{km\,s^{-1}}$, we find for the full sample (K and M together)

$$\langle v \rangle = -15.26\,\mathrm{km\,s^{-1}}. \quad (9)$$

On the other hand, if we adopt the parameter $k = 80 \pm 5\,\mathrm{km\,s^{-1}}$ from the asymmetric drift equation of Dehnen & Binney (1998), we find

$$\langle v \rangle = -\sigma_U^2/k = -14.9 \pm 1.3\,\mathrm{km\,s^{-1}}. \quad (10)$$

This independent estimate of $\langle v \rangle$ is in accordance with (9) and our values of $\langle V \rangle$ and σ_U^2 are thus in good agreement with this value of k.

As we already noticed, the M giants are a little bit older than the K giants on average and we thus expect the velocity dispersions of the subsample of M giants to be higher. We find

$$\sigma_U(\mathrm{M\ giants}) = 35.95 \pm 1.6\,\mathrm{km\,s^{-1}}, \quad (11)$$

and

$$\sigma_U(\mathrm{K\ giants}) = 34.32 \pm 0.48\,\mathrm{km\,s^{-1}}. \quad (12)$$

As expected, the difference is not very large, and the radial velocity dispersions for the two subsamples satisfy the asymmetric drift Eq. (10).

The mixed components of the velocity dispersion tensor involving vertical motions vanish within their errors. Nevertheless, the mixed component in the plane, that we denote σ_{UV}^2, is non-zero: this is not allowed in an axisymmetric Galaxy and is further discussed in Sect. 3.3. We obtain

$$\sigma_{UV}^2 = 134.26 \pm 13.28\,\mathrm{km^2\,s^{-2}} \quad (13)$$

where the error corresponds to the 15 and 85 percentiles of the correlation coefficient, assuming that the sample of U, V velocities is drawn from a two-dimensional Gaussian distribution.

In order to parametrize the deviation from dynamical axisymmetry, a useful quantity is the vertex deviation l_v, i.e., the angle one has to rotate the (U, V) coordinate system in order to diagonalize the velocity dispersion tensor. The value of the vertex deviation for our sample is

$$l_v \equiv 1/2 \arctan\left(2\sigma_{UV}^2/(\sigma_U^2 - \sigma_V^2)\right) = 10.85^\circ \pm 1.62^\circ. \quad (14)$$

This vertex deviation for giant stars is not in accordance with a perfectly axisymmetric Galaxy and could be caused by non-axisymmetric perturbations in the solar neighbourhood, or by a deviation from equilibrium (i.e. moving groups due to inhomogeneous star formation, following the classical theory of moving groups). A hint to the true nature of this vertex deviation could be the local anomaly in the UV-plane, the so-called u-anomaly (e.g. Raboud et al. 1998). If we calculate the mean velocity $\langle U \rangle$ of the stars with $V < -35\,\mathrm{km\,s^{-1}}$, we find that it is largely negative ($\langle U \rangle = -22\,\mathrm{km\,s^{-1}}$). It denotes a global outward radial motion of the stars that lag behind the galactic rotation. We see in Fig. 7 that this anomaly is due to a clump located at $U \simeq -35$ km s^{-1}, $V \simeq -45$ km s^{-1},

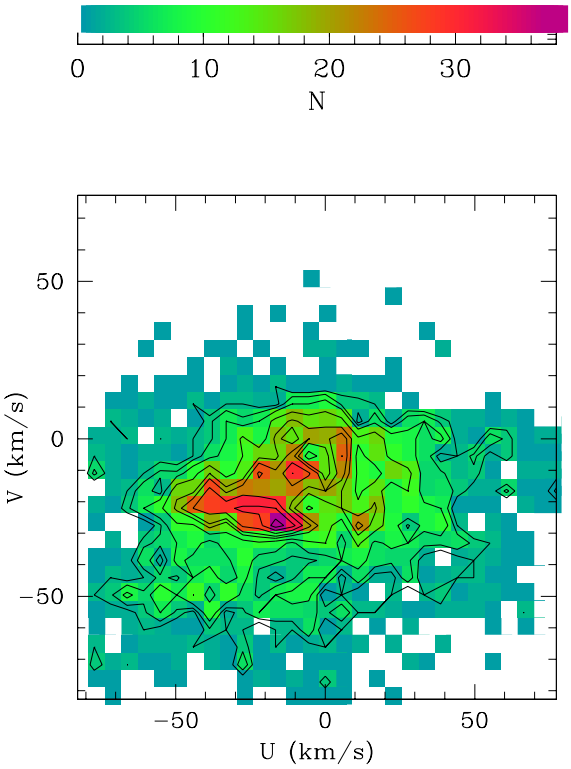

Fig. 7. Density of stars with precise parallaxes ($\sigma_\pi/\pi \leq 20\%$) in the UV-plane. The colours indicate the number of stars in each bin. The contours indicate the bins with 3, 4, 7, 12, 17, 20, 25, 30, 35 and 40 stars respectively. The concentration of stars around $U \simeq -35$ km s^{-1}, $V \simeq -45$ km s^{-1} contributes largely to the vertex deviation, while other peaks already identified by Dehnen (1998) at $U = -40$ km s^{-1}, $V = -25$ km s^{-1} (Hyades supercluster), at $U = 10$ km s^{-1}, $V = -5$ km s^{-1} (Sirius moving group), and at $U = -15$ km s^{-1}, $V = -25$ km s^{-1} (Pleiades supercluster) are also present.

the already known "Hercules" stream (Fux 2001). On the other hand, Fig. 7 reveals in fact a rich small-scale structure in the UV-plane, with several clumps which can be associated with known kinematic features: we clearly see small peaks at $U = -40$ km s^{-1}, $V = -25$ km s^{-1} (corresponding to the Hyades supercluster), at $U = 10\,\mathrm{km\,s^{-1}}$, $V = -5\,\mathrm{km\,s^{-1}}$ (Sirius moving group), and at $U = -15$ km s^{-1}, $V = -25$ km s^{-1} (Pleiades supercluster). More precise values for these peaks will be given in Sect. 3.3 where their origin will also be discussed.

3.2. Monte Carlo simulation

To reduce the bias introduced by the non-linearity of the parallax-distance transformation, the results discussed in the previous Section were obtained by restricting the sample to stars with a relative parallax error smaller than 20%. In this section, we use all the available stars, without any parallax truncation, but perform a Monte-Carlo simulation to properly evaluate the errors and biases on the kinematic parameters.

We constructed synthetic samples by drawing the stellar parallax from a Gaussian distribution centered on the *observed*

parallax value for the corresponding star, and with a dispersion corresponding to the uncertainty on the observed parallax. Note that this procedure is not strictly correct, as the Gaussian distribution should in fact be centered on the (unknown) *true* parallax. To overcome this difficulty, a fully Bayesian approach will be applied in yet another analysis of the data, as described next in Sect. 3.3.

Some a priori information has nevertheless been included to truncate the Gaussian parallax distribution in the present Monte Carlo approach, since the giant stars in our sample should not be brighter than $M_{Hp} = -2.5$ (see Figs. 12–14, 16). That threshold has been increased to $M_{Hp} = -5$ (see Fig. 10) for the stars flagged as supergiants. This prescription thus corresponds to assigning a minimum admissible parallax $\pi_{\min}$ to any given star. It prevents the situation in which very small parallaxes drawn from the Gaussian distribution yield unrealistically large space velocities. The parallax distribution used in the Monte Carlo simulation is thus

$$P(\pi) = \frac{1}{(2\Pi)^{1/2}\sigma_{\pi_{\rm obs}}} \exp\left(-\frac{1}{2}\left(\frac{\pi-\pi_{\rm obs}}{\sigma_{\pi_{\rm obs}}}\right)^2\right) \quad \text{if } \pi \geq \pi_{\min} \qquad (15)$$

$$P(\pi) = 0 \qquad \text{if } \pi < \pi_{\min}. \qquad (16)$$

The mean space velocities and the velocity dispersions are calculated for each simulated sample, and finally we adopt the average of these values (of the mean velocities and of the velocity dispersions) over 4000 simulated samples as the best estimate of the true kinematic parameters.We thus obtain:

$$\begin{aligned} \langle U\rangle &= -10.25 \pm 0.15\,{\rm km\,s^{-1}} \\ \langle V\rangle &= -22.81 \pm 0.15\,{\rm km\,s^{-1}} \\ \langle W\rangle &= -7.98 \pm 0.09\,{\rm km\,s^{-1}}. \end{aligned} \qquad (17)$$

If there is no net radial and vertical motion in the solar neighbourhood (see however Sect. 3.3.6), we may write $U_\odot = -\langle U\rangle$ and $W_\odot = -\langle W\rangle$. The results given by Eq. (17) are very close to those estimated from stars with relative errors on the parallax smaller than 20% (see Eq. (5)). They are in agreement with the values derived by Dehnen & Binney (1998) on the basis of Hipparcos proper motions of main sequence stars ($U_\odot = 10.00 \pm 0.36\,{\rm km\,s^{-1}}$, $W_\odot = 7.17 \pm 0.38\,{\rm km\,s^{-1}}$). The value of $U_\odot$ is not in perfect accordance with the one derived by Brosche et al. (2001), who found $U_\odot = 9.0 \pm 0.5\,{\rm km\,s^{-1}}$ from photometric distances and Hipparcos proper motions of K0-5 giants, nor with the one derived by Zhu (2000) who found $U_\odot = 9.6 \pm 0.3\,{\rm km\,s^{-1}}$ with the same stars as ours but without the radial velocity data. The value of $W_\odot$ contradicts slightly the one derived by Bienaymé (1999), who found $W_\odot = 6.7 \pm 0.2\,{\rm km\,s^{-1}}$ from Hipparcos proper motions. Nevertheless, these considerations on the solar motion are not very useful since we stress in Sect. 3.3.6 that the motion of the Sun is difficult to derive anyway because there are conceptual uncertainties on the mean motion of stars in the solar neighbourhood.

For the velocity dispersions, we find

$$\begin{aligned} \sigma_U &= 40.72 \pm 0.58\,{\rm km\,s^{-1}} \\ \sigma_V &= 32.23 \pm 1.41\,{\rm km\,s^{-1}} \\ \sigma_W &= 22.55 \pm 0.95\,{\rm km\,s^{-1}}. \end{aligned} \qquad (18)$$

These velocity dispersions are somewhat larger than those found for the restricted sample (8), which is not surprising since 60% of the high-velocity stars (as identified in Sect. 3.3.6) are not present in the sample restricted to the most precise parallaxes. Regarding the asymmetric drift and the slightly larger age of the M giants, the Monte Carlo method and the analysis of the restricted sample reach the same conclusion.

Concerning the mixed component of the velocity dispersion tensor in the plane, we find

$$\sigma^2_{UV} = 188.23 \pm 40.9\,{\rm km^2\,s^{-2}} \qquad (19)$$

which leads to a clearly non-zero vertex deviation of

$$l_v \equiv 1/2 \arctan\left(2\sigma^2_{UV}/(\sigma^2_U - \sigma^2_V)\right) = 16.2^\circ \pm 5.6^\circ. \qquad (20)$$

Interestingly, Soubiran et al. (2003) found no vertex deviation for low-metallicity stars in the disk, and concluded that this was consistent with an axisymmetric Galaxy: this is absolutely not the case for our sample of late-type giants. Furthermore, the value we find for the vertex deviation is larger than the one derived for late-type stars by Dehnen & Binney (1998), who showed that the vertex deviation drops from 30° for young stellar populations (probably due to young groups concentrated near the origin of the UV-plane, see also Sect. 3.3.7) to a constant value of 10° for older populations. Bienaymé (1999) also found from Hipparcos proper motions a vertex deviation of 9.2° for the giant stars. We conclude from our sample that the vertex deviation is significantly non-zero: we suggest a possible origin for this vertex deviation (which could be the same origin as for the vertex deviation of younger populations) in Sect. 3.3.7.

3.3. Bayesian approach

To obtain the kinematic characteristics of our sample in a more rigorous way, we have applied the Luri-Mennessier (LM) method described in detail by Luri (1995) and Luri et al. (1996). The starting point of this method is a model describing the basic morphological characteristics we can safely expect from the sample (spatial distribution, kinematics and absolute magnitudes), and a model of the selection criteria used to define the sample. These models are used to build a distribution function (DF) intended to describe the observational characteristics of the sample. The a priori distribution function adopted is a linear combination of partial DFs, each of which describes a group of stars (called "base group"). Each partial DF combines a kinematic model (the velocity ellipsoid introduced by Schwarzschild 1907) with a Gaussian magnitude distribution, and an exponential height distribution uncorrelated with the velocities. The phenomenological model adopted is obviously not completely rigorous, but has the advantage of being able to identify and quantify the different subgroups present in the data and possibly related to extremely complex dynamical phenomema, which cannot be easily parametrized.

The values of the parameters of the DF can be determined from the sample using a Bayesian approach: the model is adjusted to the sample by a maximum likelihood fit of the parameters. The values of the parameters so obtained provide the best representation of the sample given the a priori models assumed.

In the following Sects. 3.3.1 and 3.3.2 we describe the ingredients of the models used in this paper. Thereafter, in Sects. 3.3.3 to 3.3.6, we present the results of the maximum likelihood fit, and we discuss in Sect. 3.3.7 the different possible physical interpretations of those results.

3.3.1. Phenomenological model

To build a phenomenological model of our sample, we assume that it is a mixture of stars coming from several "base groups". A given group represents a fraction w_i of the total sample and its characteristics are described by the following components:

- *Spatial distribution*: An exponential disk of scale height Z_0 in the direction perpendicular to the galactic plane

$$\varphi_{\rm e}(d,l,b) = \exp\left(-\frac{|d\sin b|}{Z_0}\right) d^2\cos b \tag{21}$$

  and a uniform distribution along the galactic plane (a realistic approximation for samples in the solar neighbourhood like ours).
- *Velocity distribution*: A Schwarzschild ellipsoid for the velocities of the stars with respect to their Local Standard of Rest (LSR):

$$\varphi_{\rm v}(U',V',W) = {\rm e}^{-\frac{1}{2}\left(\frac{U'}{\sigma_{U'}}\right)^2-\frac{1}{2}\left(\frac{V'}{\sigma_{V'}}\right)^2-\frac{1}{2}\left(\frac{W-W_0}{\sigma_{\rm W}}\right)^2} \tag{22}$$

  where

$$\begin{aligned} U' &= (U-U_0)\cos l_v - (V-V_0)\sin l_v \\ V' &= (U-U_0)\sin l_v + (V-V_0)\cos l_v \end{aligned} \tag{23}$$

  and where l_v is the vertex deviation.
- *Galactic rotation*: An Oort-Lindblad rotation model at first order, where the rotation velocity is added to the mean LSR velocity (given by the Schwarzschild ellipsoid above). The same values were adopted for the Oort constants as in Sects. 3.1 and 3.2
- *Luminosity*: We have adopted a Gaussian distribution for the absolute magnitudes of the stars:

$$\varphi_{\rm M}(M) = \exp\left(-\frac{1}{2}\left(\frac{M-M_0}{\sigma_{\rm M}}\right)^2\right). \tag{24}$$

  This is just a first rough approximation. A better model would include a dependence of the absolute magnitude on a colour index but is more complex (we leave it for future papers).
- *Interstellar absorption*: In the LM method, the correction of interstellar absorption is integrated in the formalism. A model, giving its value as a function of the position (d,l,b), is needed: the Arenou et al. (1992) model has been chosen here.

The DF of each base group is simply the product of the space, velocity and magnitude distributions presented here, with different values for the model parameters. The total distribution function $\mathcal{D}$ of the sample is a linear combination of the partial DFs of the different base groups.

Both the relative fractions of the different base groups and the model parameters will be determined using a Maximum Likelihood fit, as described in Sect. 3.3.3. However, the number of groups ($n_{\rm g}$) composing our sample is not known a priori. A likelihood test – like Wilk's test, Soubiran et al. (1990) – will be used to determine it: ML estimations are performed with $n_{\rm g} = 1, 2, 3, \ldots$ and the maximum likelihoods obtained for each case are compared using the test to decide on the most likely value of $n_{\rm g}$.

3.3.2. Observational selection and errors

As pointed out above, the correct description of the observed characteristics of the sample requires that its selection criteria be included in the model. In our case, our sample of giants (like the Hipparcos Catalogue as a whole) is composed primarily of stars belonging to the Hipparcos *survey* plus stars added on the basis of several heterogeneous criteria.

In the case of the Hipparcos survey, the selection criteria are just based on the apparent V magnitude. For a given line of sight, with galactic latitude b, the survey is complete up to

$$V = 7.3 + 1.1|\sin b|. \tag{25}$$

In our case, the $H_{\rm p}$ Hipparcos magnitude has been used instead of V. Therefore the survey stars in our sample will follow a similar "completeness law" in $H_{\rm p}$ that we have adopted to be approximately

$$H_{\rm p} = 7.5 + 1.1|\sin b| \tag{26}$$

assuming an average $H_{\rm p} - V$ of 0.2 mag for the stars in our sample.

This law, altogether with the cutoff in declination ($\delta > 0°$), allows us to quite realistically model the selection of the survey stars in the sample, but leaves out 10% of the total sample. In order to be able to use the full sample, we must define the selection of the non-survey stars as well, as (approximately) done by the following completeness law:

- Completeness linearly decreasing from 1 at $H_{\rm p} = 7.5 + 1.1|\sin b|$ down to zero at $H_{\rm p} = 11.5$

This condition together with the completeness up to $H_{\rm p} = 7.5 + 1.1|\sin b|$, and with the cutoff in declination, defines the selection of the complete sample.

The individual errors on the astrometric and photometric data are also taken into account in the model. We assume that the observed values are produced by Gaussian distributions of observational errors around the "true" values, with standard deviations given by the errors quoted in the Hipparcos Catalogue, the Tycho-2 catalogue or the CORAVEL database.

In the end, we can define for each star a joint distribution function of the true and observed values:

$$\mu(\boldsymbol{x},\boldsymbol{z}||\boldsymbol{\theta}) = \mathcal{D}(\boldsymbol{x}||\boldsymbol{\theta})\,\epsilon(\boldsymbol{z}||\boldsymbol{x})\,S(\boldsymbol{z}) \tag{27}$$

where $\boldsymbol{x}$ are the true values (position in the LSR, velocities with respect to the LSR, absolute magnitude), $\boldsymbol{z}$ the observed values (position on the sky, parallax, proper motions, radial

Table 1. Maximum-Likelihood parameters obtained using 5177 survey stars only. The number of stars belonging to each group (as listed in Col. 34 of Table A.1) is given in the last row. Although obtained from the assignment process described in Sect. 3.3.4, it is *not,* strictly, a ML-parameter, in contrast to the "fraction" w_i ($i = 1, ...6$) of the whole sample belonging to the considered group, as listed in the previous row. Therefore, the observed fraction of stars in each group could be slightly different from the true fraction w_i of that group in the entire population.

	Group Y	Group HV	Group HyPl	Group Si	Group He	Group B
M_0 (mag)	0.61 ± 0.91	2.21 ± 0.22	1.15 ± 0.37	1.08 ± 0.57	1.27 ± 0.37	1.23 ± 0.17
σ_M (mag)	1.85 ± 0.24	1.29 ± 0.10	0.88 ± 0.21	1.16 ± 0.24	0.88 ± 0.12	1.05 ± 0.08
U_0 (km s^{-1})	−11.63 ± 2.30	−17.56 ± 3.46	−31.23 ± 0.99	5.19 ± 3.03	−42.09 ± 4.76	−2.92 ± 1.54
$\sigma_{U'}$ (km s^{-1})	15.61 ± 1.22	53.45 ± 2.14	11.46 ± 1.53	13.48 ± 2.66	26.08 ± 13.13	31.82 ± 1.56
V_0 (km s^{-1})	−11.57 ± 2.08	−43.96 ± 3.20	−20.00 ± 0.75	4.22 ± 1.95	−50.60 ± 4.67	−15.15 ± 2.36
$\sigma_{V'}$ (km s^{-1})	9.44 ± 1.36	36.14 ± 1.79	4.89 ± 1.10	4.59 ± 4.22	8.62 ± 3.03	17.60 ± 0.78
W_0 (km s^{-1})	−7.79 ± 0.95	−7.76 ± 2.30	−4.82 ± 1.85	−5.57 ± 2.13	−6.94 ± 3.56	−8.16 ± 0.91
σ_W (km s^{-1})	6.94 ± 0.78	32.54 ± 1.54	8.76 ± 1.08	9.43 ± 2.23	16.66 ± 1.62	16.26 ± 0.77
Z_0 (pc)	73.44 ± 6.33	901.04 ± 440.13	128.70 ± 19.21	149.43 ± 23.67	201.80 ± 55.24	196.05 ± 12.34
l_v (°)	17.07 ± 5.81	0.22 ± 4.89	−5.65 ± 4.59	−14.17 ± 25.28	−5.67 ± 11.16	−0.22 ± 5.21
Fraction w	0.086 ± 0.013	0.149 ± 0.022	0.071 ± 0.007	0.050 ± 0.030	0.065 ± 0.017	0.579 ± 0.047
Number of stars	345	505	334	204	372	3417

velocity, apparent magnitude), $\boldsymbol{\theta}$ the set of parameters of the model, S the selection function taking into account the selection criteria of the sample, and ϵ the Gaussian distribution of observational errors.

For each star, we can then easily deduce the distribution function of the observed values:

$$O(z||\boldsymbol{\theta}) = \int \mu(\boldsymbol{x}, z||\boldsymbol{\theta})\, \mathrm{d}\boldsymbol{x}. \tag{28}$$

The fact that the selection function and the error distribution are taken into account in this distribution function prevents from all the possible biases.

3.3.3. Maximum likelihood

The principle of maximum likelihood (ML) can be briefly described as follows: let $\boldsymbol{z}$ be the random variable of the observed values following the density law given by $O(z||\boldsymbol{\theta}_0)$, where $\boldsymbol{\theta}_0 = (w_1, M_{0_1}, \sigma_{M_1}, U_{0_1}, \sigma_{U'_1}, V_{0_1}, \sigma_{V'_1}, W_{0_1}, \sigma_{W_1}, Z_{0_1}, l_{v_1}, w_2, \ldots, l_{v_{n_g}})$ is the set of unknown parameters on which it depends.

The *Likelihood Function* is defined as

$$\mathcal{L}(\boldsymbol{\theta}) = \prod_{i=1}^{n_*} O(z_i||\boldsymbol{\theta}). \tag{29}$$

The value of $\boldsymbol{\theta}$ which maximizes this function is the ML estimator, $\boldsymbol{\theta}_{\mathrm{ML}}$, of the parameters $\boldsymbol{\theta}_0$ characterizing the density law of the sample. It can be shown that $\boldsymbol{\theta}_{\mathrm{ML}}$ is asymptotically non-biased, asymptotically Gaussian and that for large samples, it is the most efficient estimator (see Kendall & Stuart 1979).

Once the ML estimator of the parameters has been found, simulated samples (generation of random numbers following the given distribution) are used to check the equations and programs developed for the estimation. They also allow a good estimation of the errors on the results and the detection of possible biases: once a ML estimation $\boldsymbol{\theta}_{\mathrm{ML}}$ has been obtained, several samples corresponding to the parameters $\boldsymbol{\theta}_{\mathrm{ML}}$ are simulated and the method is applied to them. The comparison of the results (which could be called "the estimation of the estimation") with the original $\boldsymbol{\theta}_{\mathrm{ML}}$ allows us to detect possible biases. The dispersion of these results $\sigma(\boldsymbol{\theta}_{\mathrm{ML}})$ can be taken as the error of the estimation.

The low maximum likelihood obtained when the full sample is modelled with a single base group indicates that the kinematic properties of giant stars in the solar neighbourhood cannot be fitted by a single Schwarzschild ellipsoid. The first acceptable solution requires three base groups: one of bright giants and supergiants with "young" kinematics (further discussed in Sect. 3.3.6), one of high-velocity stars and finally one group of "normal" stars. This third group exhibits plenty of small-scale structure, and this small-scale structure can be successfully modelled by 3 more base groups (leading to a total of 6 groups in the sample, called groups Y, HV, HyPl, Si, He, and B, further discussed in Sect. 3.3.6). These supplementary groups are statistically significant, as revealed by a Wilks test. Statistically, solutions with 7 or 8 groups are even better, but these solutions are not stable anymore and are thus not useful (they depend too much on the observed values of some individual stars). Table 1 lists the values of the ML parameters for a model using just the 5177 (out of 5397) survey stars that comply with the completeness law (Eq. (26)). Table 2 lists those values for a model using the whole sample of 6030 stars with our modified selection law. The models for the survey stars alone and for the whole sample give very similar results (except for the scale height Z_0 of group HV – see Sect. 3.3.6 – which is not well constrained since our sample does not go far enough above the galactic plane), thus providing a strong indication that the results for the whole sample are reliable. The errors

Table 2. Same as Table 1 for the full sample of 6030 stars.

	Group Y	Group HV	Group HyPl	Group Si	Group He	Group B
M_0 (mag)	0.68 ± 0.25	2.04 ± 0.23	0.95 ± 0.13	0.87 ± 0.19	1.21 ± 0.18	1.04 ± 0.07
σ_M (mag)	1.78 ± 0.06	1.43 ± 0.08	0.74 ± 0.10	1.12 ± 0.08	0.95 ± 0.09	1.07 ± 0.03
U_0 (km s^{-1})	−10.41 ± 0.94	−18.50 ± 2.82	−30.34 ± 1.54	6.53 ± 1.93	−42.13 ± 1.95	−2.78 ± 1.07
$\sigma_{U'}$ (km s^{-1})	15.37 ± 1.09	58.02 ± 1.87	11.83 ± 1.34	14.37 ± 2.05	28.35 ± 1.68	33.30 ± 0.70
V_0 (km s^{-1})	−12.37 ± 0.90	−53.30 ± 3.10	−20.27 ± 0.62	3.96 ± 0.67	−51.64 ± 1.07	−15.42 ± 0.82
$\sigma_{V'}$ (km s^{-1})	9.93 ± 0.75	41.36 ± 1.70	5.08 ± 0.76	4.63 ± 0.71	9.31 ± 1.22	17.94 ± 0.80
W_0 (km s^{-1})	−7.75 ± 0.57	−6.61 ± 1.82	−4.82 ± 0.80	−5.80 ± 1.15	−8.06 ± 1.30	−8.26 ± 0.38
σ_W (km s^{-1})	6.69 ± 0.58	39.14 ± 1.69	8.75 ± 0.74	9.66 ± 0.82	17.10 ± 1.63	17.65 ± 0.34
Z_0 (pc)	80.27 ± 6.18	208.08 ± 27.89	106.27 ± 14.37	127.96 ± 19.65	132.89 ± 9.42	141.21 ± 5.20
l_v (°)	16.40 ± 10.26	0.16 ± 4.77	−8.79 ± 4.05	−11.96 ± 3.53	−6.53 ± 2.77	−2.18 ± 1.60
Fraction w	0.096 ± 0.008	0.106 ± 0.010	0.070 ± 0.008	0.053 ± 0.009	0.079 ± 0.009	0.596 ± 0.015
Number of stars	413	401	392	268	529	4027

on the parameters listed in Tables 1 and 2 are the dispersions coming from the simulated samples.

3.3.4. Group assignment

The probabilities for a given star to belong to the various groups is provided by the LM method, and the most probable group along with the corresponding probability is listed in Table A.1. Indeed, let w_j be the a priori probability (i.e. the ML parameter of Table 2) that a star belongs to the jth group and $O_j(z \mid \boldsymbol{\theta}_j)$ the distribution of the observed quantities z in this group (deduced from the phenomenological model adopted and depending on the parameters $\boldsymbol{\theta}_j$ of this model for the group). Then, using Bayes formula, the a posteriori probability for a star to belong to the jth group given its measured values z_* is:

$$P(* \in G_j \mid z_*) = \frac{w_j O(z_* | \boldsymbol{\theta}_j)}{\sum_{k=1}^{n_g} w_k O(z_* | \boldsymbol{\theta}_k)}. \quad (30)$$

Using this formula the a posteriori probabilities that the star belongs to a given group can be compared, and the star can be assigned to the most likely one (Table A.1).

Note that this procedure, like any method of statistical classification, will have a certain percentage of misclassifications. However, the reliability of each assignment is clearly indicated by the probability given in Col. 35 of Table A.1.

3.3.5. Individual distance estimates

Once a star has been assigned to a group, and given the ML estimator of the group parameters and the observed values for the star z_*, one can obtain the marginal probability density law $\mathcal{R}(d)$ for the distance of the star from the global probability density function.

This can then be used to obtain the expected value of the distance

$$\overline{d} = \int_0^\infty d\,\mathcal{R}(d)\,\mathrm{d}d \quad (31)$$

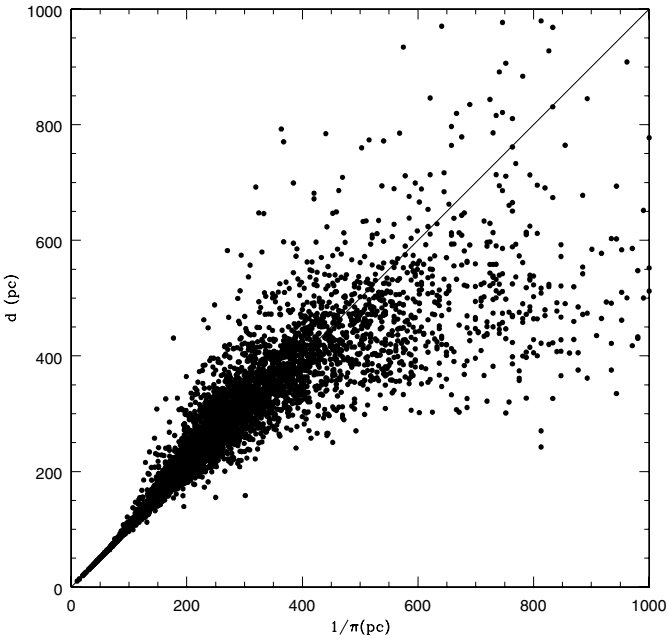

Fig. 8. Comparison of the (biased) distances obtained from a simple inversion of the parallax, and the maximum-likelihood distances $\overline{d}$ obtained from the LM method.

and its dispersion

$$\epsilon_d^2 = \int_0^\infty (d - \overline{d})^2\,\mathcal{R}(d)\,\mathrm{d}d. \quad (32)$$

The first can be used as a distance estimator free of biases and the second as its error (Cols. 28 and 29 of Table A.1). Figure 8 reveals that the biases in the distance derived from the inverse parallax are a combination of those resulting from truncations in parallax and apparent magnitude as discussed in Luri & Arenou (1997).

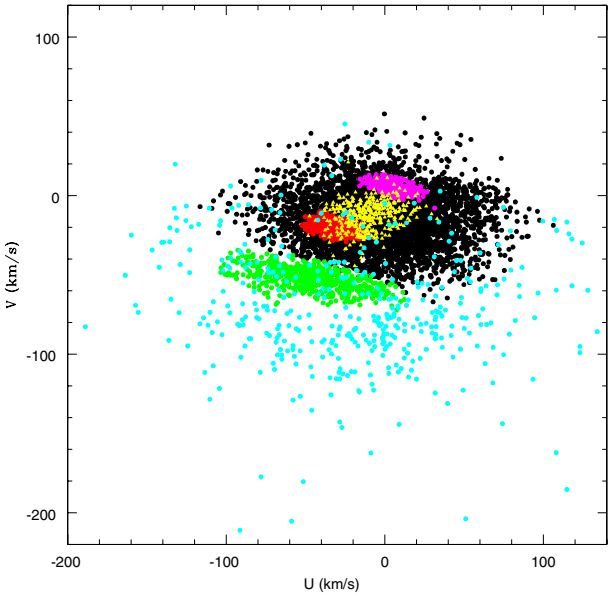

Fig. 9. All the stars plotted in the UV-plane with their values of U and V deduced from the LM method. The 6 different groups are represented in this figure: group Y in yellow, group HV in blue, group HyPl in red, group Si in magenta, group He in green and group B in black. Note that the yellow group (Y) extends just far enough to touch both the red (HyPl) and magenta (Si) groups.

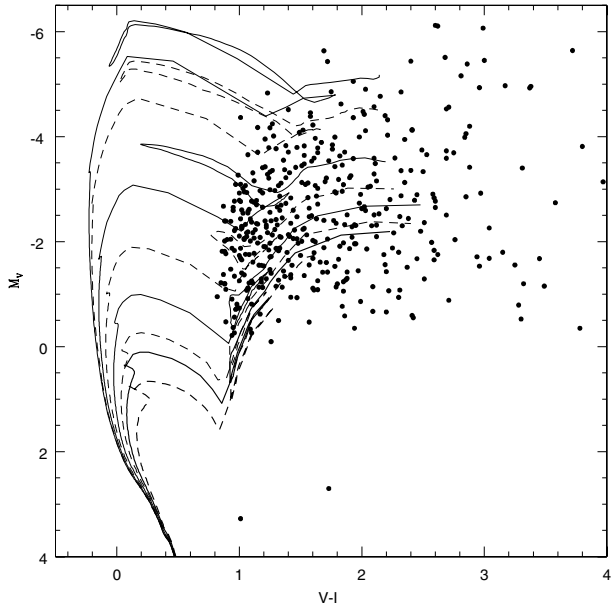

Fig. 10. HR diagram of group Y. The absolute magnitude used here is M_V. Isochrones of Lejeune & Schaerer (2001) for $Z = 0.008$ and $\log(\text{age(yr)}) = 7.4, 7.6, 8, 8.3, 8.55, 8.75, 8.85, 9$. $V - I$ indices were computed from the colour transformation of Platais et al. (2003).

3.3.6. The various groups present in the sample

We have plotted in Fig. 9 the stars in the UV-plane by using the expected values of U and V deduced from the LM method. The 6 different groups are represented in this figure. The structure of the UV-plane is similar to the one already identified (in Fig. 7) for the stars with precise parallaxes ($\sigma_\pi/\pi \leq 20\%$). This similarity is a strong indication that the subgroups identified by the LM method are not artifacts of this method. Several groups can be identified with known kinematic features of the solar neighbourhood.

Group Y: *The young giants*

The first group is one with "young" kinematics (yellow group in Fig. 9), with a small velocity dispersion and with a vertex deviation of $l_v = 16.4°$. Quite remarkably, the value of $\langle M_{H\mathrm{p}} \rangle$ for this group is 0.68 (see Table 2), the brightest among the 6 groups. An important property of this group is thus its young kinematics coupled with its large average luminosity: the most luminous giants and supergiants[1] in our sample thus appear to have a small dispersion in the UV-plane, in agreement with the general idea that younger, more massive giants are predominantly found at larger luminosities in the Hertzsprung-Russell diagram and are, at the same time, concentrated near the origin of the UV-plane. It must be stressed that nothing in the LM method can induce such a correlation between velocities and luminosity artificially. This result must thus be considered as a robust result, even more so since the group Y of young giants was present in all solutions, irrespective of the number of groups imposed. This group is centered on the usual antisolar motion (Dehnen & Binney 1998) in U and W as seen in Table 2.

Figure 10 locates stars from group Y in the HR diagram, constructed from the $V - I$ colour index as provided by the colour transformation of Platais et al. (2003), based on the *measured* $H_\mathrm{p} - V_\mathrm{T2}$ colour index (and is thus more accurate than the Hipparcos $V - I$ index; see Appendix for more details). The isochrones of Lejeune & Schaerer (2001), for a typical metallicity $Z = 0.008$, indicate that the age of stars from group Y is of the order of several 10^6 to a few 10^8 yr.

The observed members of group Y, as displayed in Fig. 10, appear to be brighter than the true average absolute magnitude for the group listed in Tables 1 and 2 ($\langle M_{H\mathrm{p}} \rangle = 0.68$) and assigned by the LM method. This is a natural consequence of the Malmquist bias (Malmquist 1936) for a magnitude-limited sample. Nevertheless, even the true average absolute magnitude makes group Y the brightest and youngest one.

Group HV: *The high-velocity stars*

This group is composed of high-velocity stars (represented in blue on Fig. 9). Those stars are probably mostly halo or thick-disk stars, even though the value of the scale height of this population is poorly constrained (hence the large difference between that parameter derived from the full sample – Table 2 – and from survey stars only – Table 1) because our sampling distance is too small: indeed Fig. 8 shows that the distance of most stars in our sample is smaller than the scale height of the thick disk (665 pc $< Z_{0,\mathrm{thick}} <$ 1000 pc). This group represents about 10% of the whole sample (Table 2, although, like Z_0, this parameter is not well constrained), and this value is consistent with the mass fraction of the thick disk relative to the thin disk in the solar neighbourhood.

Going back to the different results obtained for the velocity dispersions in Eqs. (8) and (18), notice that 247 stars (out

[1] Almost all stars a priori flagged as supergiants (see Sects. 2.2, 3.2 and Fig. 5) do belong to group Y.

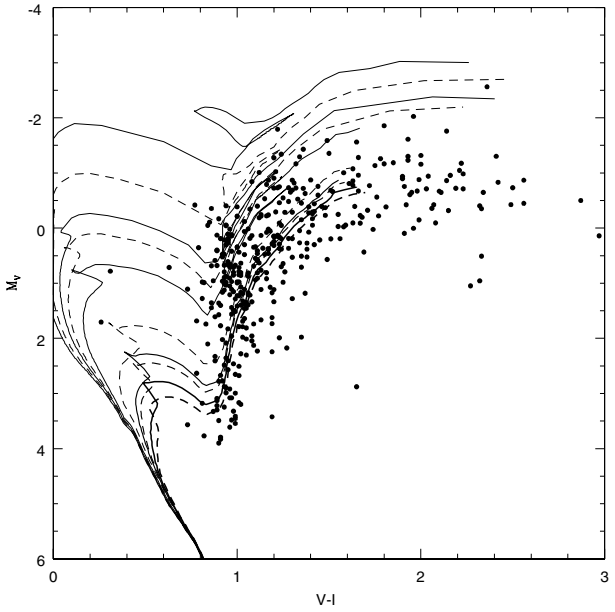

Fig. 11. HR diagram of group HV. Isochrones of Lejeune & Schaerer (2001) for $Z = 0.008$ and $\log(\text{age(yr)}) = 8.3, 8.55, 8.75, 8.85, 9, 9.3, 9.45. 9.5, 9.6, 9.7$. $V - I$ indices were computed from the colour transformation of Platais et al. (2003).

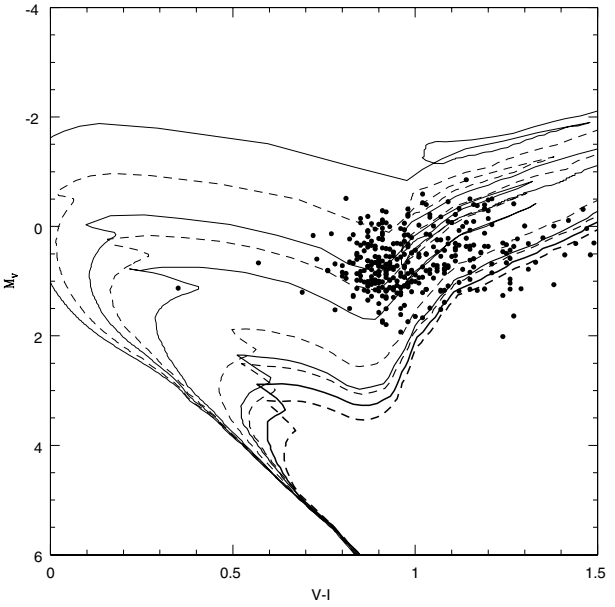

Fig. 12. HR diagram of group HyPl. Isochrones of Lejeune & Schaerer (2001) for $Z = 0.02$ and $\log(\text{age(yr)}) = 8.3, 8.55, 8.75, 8.85, 9, 9.3, 9.45. 9.5, 9.6, 9.7$. We calculated $V - I$ using the colour transformation of Platais et al. (2003). The stars at the bottom-right of the diagram could be very old metal rich stars (in contradiction with the age-metallicity relation which is obviously not correct if no other factors are taken into account).

of 401) of this group have relative errors on their Hipparcos parallax higher than 20%.

We clearly see in Fig. 11 that stars of this group are old, mostly older than 1 Gyr and it seems clear that some stars at the bottom of the HR diagram are as old as the Galaxy itself. It is also striking that the envelope of this kinematically "hot" group seems to correspond to a portion of a circle approximately centered on a zero-velocity frame with respect to the galactic center, and with a radius of the order of 280 km s^{-1}. We refrain, however, from providing numerical values for the position of this circular envelope in the UV-plane, because of the rather limited number of stars defining this limit and the absence of antirotating halo stars in our sample. Note that a lower limit to the local escape velocity is provided by the velocity $(U^2 + (V + 220)^2 + W^2)^{1/2} = 281$ km s^{-1} of HIP 89298, the fastest star in group HV.

The detection of this group of high-velocity stars "cleans" the sample and allows us to study the fine structure of the velocity distribution of disk stars.

Group HyPl: *Hyades-Pleiades supercluster*

The group represented in red in Fig. 9 occupies the well-known region of the Hyades and Pleiades superclusters. The large spatial dispersion of the HyPl stars clearly hints at their supercluster rather than cluster nature, since they are spread all over the sky with a wide range of distances (up to 500 pc). The Hyades ($\langle U\rangle = -40$ km s^{-1}, $\langle V\rangle = -25$ km s^{-1}, see Dehnen 1998) and Pleiades ($\langle U\rangle = -15$ km s^{-1}, $\langle V\rangle = -25$ km s^{-1}, see Dehnen 1998) superclusters are known since Eggen (1958, 1975). It was also noticed (Eggen 1983) that several young clusters (NGC 2516, IC 2602, α Persei) have the same V-component as those superclusters. We obtain $\langle V\rangle = -20.3$ km s^{-1}for our supercluster structure, and thus refine the old value $\langle V\rangle = -25$ km s^{-1}, with in addition the fact that the group is tilted in the anti-diagonal direction of the UV-plane, i.e., it has a negative vertex deviation ($l_v = -8.7°$). The concept of branches in the UV-plane (Skuljan et al. 1999), of quasi-constant V but slightly tilted in the anti-diagonal direction, will be further discussed below in relation to the other groups.

Metallicity is available for 17 stars of the HyPl group (McWilliam 1990), and it is interesting to note that the average metallicity seems to be close to solar ([Fe/H] = 0; Fig. 15) as already noticed by Chereul & Grenon (2001). This is quite unusual for giant stars. The metallicity of the stars from group B for example is centered on [Fe/H] = −0.2. Plotting the HyPl stars in a HR diagram (Fig. 12) and using the solar-metallicity isochrones of Lejeune & Schaerer (2001) reveals that the stars forming the HyPl group are by far not coeval (despite the fact that HyPl stars have a smaller age spread than the Si and He groups discussed below, especially because the HyPl group is lacking young supergiants). Although a precise determination of the ages of HyPl stars would require the knowledge of their metallicities, it seems nevertheless clear that there are a lot of clump stars with ages reaching 1 Gyr, and that there are clearly stars older than 2 Gyr, in sharp contrast to the ages of about 80 and 600 Myr for the Pleiades and Hyades clusters themselves. This result of age heterogeneity, already noticed by Chereul & Grenon (2001) for the Hyades supercluster, is an important clue to identify the origin of supercluster-like structures, as discussed in Sect. 3.3.7.

Finally, the value $\langle W\rangle = -4.8 \pm 0.8$ km s^{-1} differs significantly from the vertical solar motion ($W_\odot = 7$ to 8 km s^{-1}; see Sects. 3.1, 3.2, and group B in Tables 1 and 2), indicating that the group has a slight net vertical motion.

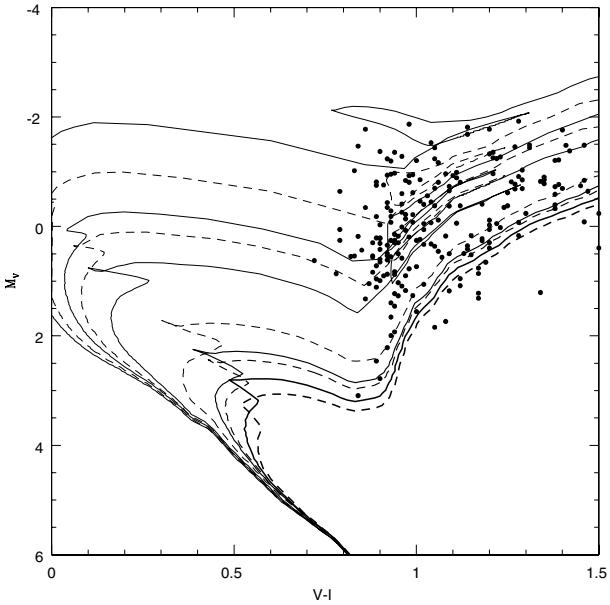

Fig. 13. HR diagram of group Si. Isochrones of Lejeune & Schaerer (2001) for $Z = 0.008$ and log (age(yr)) = 8.3, 8.55, 8.75, 8.85, 9, 9.3, 9.45. 9.5, 9.6, 9.7.

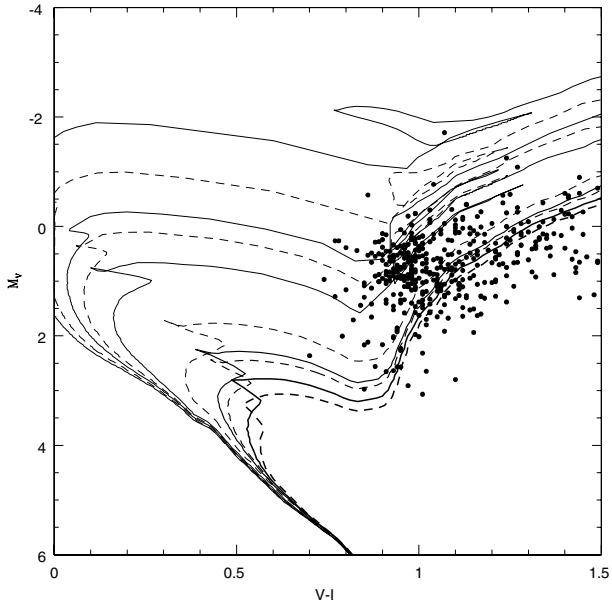

Fig. 14. HR diagram of group He. Isochrones of Lejeune & Schaerer (2001) for $Z = 0.008$ and log (age(yr)) = 8.3, 8.55, 8.75, 8.85, 9, 9.3, 9.45. 9.5, 9.6, 9.7.

Group Si: *Sirius moving group*

The Sirius moving group (represented in magenta in Fig. 9) is known since Eggen (1958, 1960) and is traditionally located at $\langle U \rangle = 10$ km s^{-1}, $\langle V \rangle = -5$ km s^{-1} (Dehnen 1998). The LM method refines those values and locates it at $\langle U \rangle = 6.5$ km s^{-1}, $\langle V \rangle = 3.9$ km s^{-1}. The spatial distribution once again indicates that this group has a supercluster-like nature. Metallicity from McWilliam (1990) is available for 12 stars of the Si group (Fig. 15). Contrarily to the situation prevailing for the HyPl group, the metallicity distribution within the Si group appears similar to that for the bulk of the giants in the solar neighbourhood, as represented by group B. Isochrones for a typical value of $Z = 0.008$ (Fig. 13) indicate that the ages are widely spread, even more so than for the HyPl group.

Group He: *Hercules stream*

The "Hercules stream" (represented in green in Fig. 9), located by the LM method at $\langle U \rangle = -42$ km s^{-1}, $\langle V \rangle = -51$ km s^{-1} has been named by Raboud et al. (1998) the u-anomaly. It corresponds to a global outward radial motion of the stars which lag behind the galactic rotation: known since Blaauw (1970), it is traditionally centered on $\langle U \rangle = -35$ km s^{-1}, $\langle V \rangle = -45$ km s^{-1} (see Fux 2001). It is strongly believed since several years that its origin is of dynamical nature, as further discussed in the next section. Once again, the Hertzsprung-Russell diagram of Fig. 14 indicates a wide range of ages in this group (for a typical value of $Z = 0.008$).

Note that the three groups HyPl, Si and He could be interpreted in term of extended branches crossing the UV-plane (Skuljan et al. 1999; Nordström et al. 2004): one is Hercules, another is the combination of Hyades and Pleiades, and the third one is Sirius. The high dispersion of the streams azimuthal (V) component confirms this view. The branches are somewhat tilted along the anti-diagonal direction. These properties could be understood in the classical theory of moving groups as discussed in next section but also in the context of a dynamical origin for the substructure.

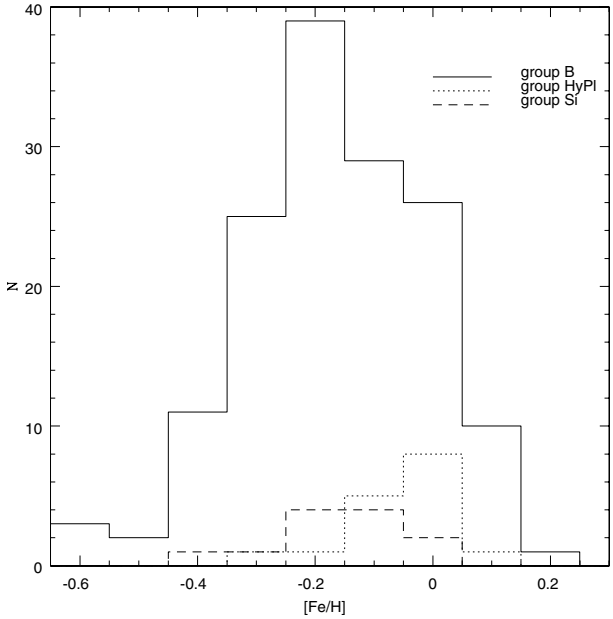

Fig. 15. Histogram of the metallicity in groups B, HyPl and Si for the stars present in the analysis of McWilliam (1990).

Group B: *Smooth background*

Most stars are part of an "axisymmetric", "smooth" background represented in black in Fig. 9. The average metallicity of this group seems to be slightly subsolar (Fig. 15) as expected for a sample of disk giants: Girardi & Salaris (2001) found an average metallicity of [Fe/H] $= -0.12 \pm 0.18$, while for their sample of F and G dwarfs, Nordström et al. (2004) found [Fe/H] $= -0.14 \pm 0.19$. Using isochrones for a typical value of $Z = 0.008$ (see Fig. 16), we see that there is a large

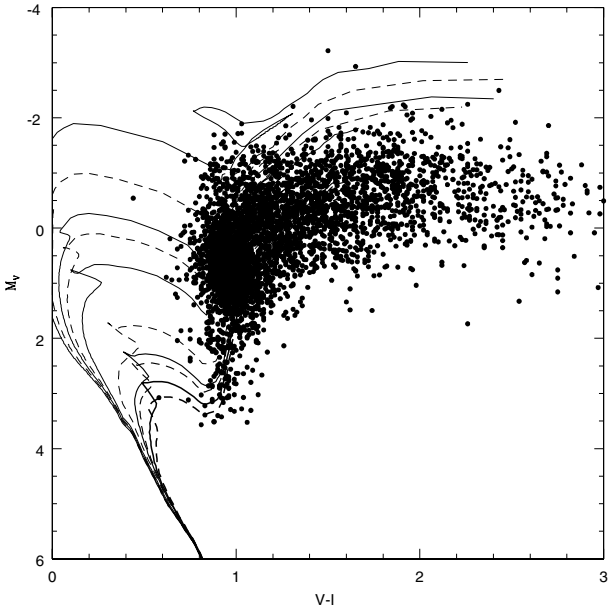

Fig. 16. HR diagram of group B. Isochrones of Lejeune & Schaerer (2001) for $Z = 0.008$ and log (age(yr)) = 8.3, 8.55, 8.75, 8.85, 9, 9.3, 9.45. 9.5, 9.6, 9.7.

spread in age. This is typical of the mixed population of the galactic disk, composed of stars born at many different epochs since the birth of the Galaxy.

In the UV-plane, the velocity ellipsoid of this group is not centered on the value commonly accepted for the antisolar motion: it is centered instead on $\langle U \rangle = -2.78 \pm 1.07$ km s^{-1}. However, the full data set (including the various superclusters) *does* yield the usual value for the solar motion (see Sect. 3.2). This discrepancy clearly raises the essential question of how to derive the solar motion in the presence of streams in the solar neighbourhood: does there exist in the solar neighbourhood a subset of stars having no net radial motion? If the smooth background is indeed an axisymmetric background with no net radial motion, we have found a totally different value for the solar motion. Nevertheless, we have no strong argument to assess that this is the case, especially if the "superclusters" have a dynamical origin, as proposed in the next section. Moreover, the group Y of young giants is centered on the commonly accepted value of $\langle U \rangle = -10.41 \pm 0.94$ km s^{-1} and this difference between groups Y and B clearly prevents us from deriving without ambiguity the solar motion. If the giant molecular clouds (GMCs) from which the young stars arose are on a circular orbit, then the $\langle U \rangle$ value of group Y is the acceptable one for the antisolar motion, but nothing proves that the GMCs are not locally moving outward in the Galaxy under the effect of the spiral pattern. No value can thus at the present time be given for the radial solar motion but only some different estimates depending on the theoretical hypothesis we make on the nature of the substructures observed in velocity space. Theoretical investigations and dynamical simulations thus appear to be the only ways to solve this problem. On the other hand, the value of $\langle W \rangle = -8.26 \pm 0.38$ km s^{-1} for group B is in accordance with the usual motion of the Sun perpendicular to the galactic disk (see Sect. 3.2), and thus seems to be a reliable value because streams have a smaller effect on the vertical motion of stars.

3.3.7. Physical interpretation of the groups: Dynamical streams?

Several mechanisms may be responsible for the substructrure observed in velocity space in the solar neighbourhood. Hereafter, we list them and confront them with the results of our kinematic study.

A first class of mechanisms is that associated with inhomogeneous star formation responsible for a deviation from equilibrium in the solar neighbourhood: this theory states that a large number of stars are formed (almost) simultaneously in a certain region of the Galaxy and create a cluster-like structure with a well-defined position and velocity. After several galactic rotations, the cluster will evaporate and form a tube called "supercluster". Stars in the "supercluster" still share common V velocities when located in the same region of the tube (for example in the solar neighbourhood) for the following reason, first put forward by Woolley (1961): if the present galactocentric radius of a star on a quasi-circular epicyclic orbit equals that of the Sun (denoted $\varpi_\odot$), and if such a star is observed with a peculiar velocity $v = V + V_\odot$, then its guiding-center radius ϖ_g writes

$$\varpi_g = \varpi_\odot - x_g = \varpi_\odot + \frac{v}{2B} \tag{33}$$

where x_g is the position of its guiding-center in the Cartesian reference frame associated with the LSR (in the solar neighbourhood approximation, the impact of y_g is negligible), and B is the second Oort constant. Woolley (1961) pointed out that disk stars (most of which move on quasi-circular epicyclic orbits) that formed at the same place and time, and that stayed together in the Galaxy after a few galactic rotations (since they are all currently observed in the solar neighbourhood) must necessarily have the same period of revolution around the Galactic center, and thus the same guiding-center ϖ_g, and thus the same velocity $V = v - V_\odot$ according to Eq. (33). This theory has thus the great advantage of predicting extended horizontal branches crossing the UV-plane (similar to those observed in our sample in Fig. 9 and already identified by Skuljan et al. 1999; and by Nordström et al. 2004, in their sample of F and G dwarfs). Moreover, it is easy to understand in this framework that the Group HyPl seems to be more metal-rich than the smooth background (see Fig. 15). However, this theory does not explain the tilt of the branches that we observe in our sample. Moreover, to explain the wide range of ages observed in those branches (see Figs. 12, 13, and also Chereul & Grenon 2001), the stars must have formed at different epochs (see e.g. Weidemann et al. 1992) out of only two large molecular clouds (one associated with the Sirius branch and another with the Hyades-Pleiades branch). Chereul et al. (1998) suggested that the supercluster-like velocity structure is just a chance juxtaposition of several cluster remnants, but this hypothesis requires extraordinary long survival times for the oldest clusters (with ages $>$ 2 Gyr) in the supercluster-like structure. This long survival time is made unlikely by the argument of

Boutloukos & Lamers (2003) who found that clusters within 1 kpc from the Sun having a mass of $m \times 10^4\ M_\odot$ can survive up to m Gyr in the Galaxy: indeed heavy clusters of more than $2 \times 10^4\ M_\odot$ are probably very rare in the *disk*.

An explanation for the wide range of ages observed in the superclusters could be the capture of some older stars by the high concentration of mass in a molecular cloud, at the time of the formation of a new group of stars (while other stars would be scattered by the molecular cloud). Though this hypothesis could be tested in N-body simulations involving gas, it would imply that the local clumps of the potential not only perturb the motion of stars but dominate it, which is in contradiction with the high predominance of the global potential on the local clumps. This explanation is thus highly unlikely too.

The second class of mechanisms involves the theory of hierarchic formation of the galaxies: following this theory, galaxies were built up by the merging of smaller precursor structures. It is known since the discovery of the absorption of the Sagittarius dwarf galaxy by the Milky Way (Ibata et al. 1994) that some streams in the Galaxy are remnants of a merger with a satellite galaxy. Helmi et al. (1999) showed that some debris streams are also present in the galactic halo near the position of the Sun. Such streams could also be present in the velocity substructure of the disk: it seems to be the case of the Arcturus group at $U \simeq 0$ km s^{-1}, $V \simeq -115$ km s^{-1}, as recently proposed by Navarro et al. (2004). In this scenario, the streams observed in our kinematic study could also be the remnants of merger events between our Galaxy and a satellite galaxy. The merger would have triggered star formation whereas the oldest giant stars would be stars accreted from the companion galaxy. A merger with a satellite galaxy would moreover induce a perturbation in W, as we observe in group HyPl in which $\langle W \rangle = -4.8 \pm 0.8$ km s^{-1}. If the hierarchical ("bottom-up") cosmological model is correct, the Milky Way system should have accreted and subsequently tidally destroyed approximately 100 low-mass galaxies in the past 12 Gyr (see Bullock & Johnston 2004), which leads to one merger every 120 Myr, but the chance that two of them (leading to the Hyades-Pleiades and Sirius superclusters) have left such important signatures in the disk near the position of the Sun is statistically unlikely (although not impossible).

The third class of mechanisms is the class of purely dynamical ones. A dynamical mechanism that could cause substructure in the local velocity distribution is the disturbing effect of a non-axisymmetric component of the gravitational potential, like the rotating galactic bar. The Hercules stream was recently identified with the bimodal character of the local velocity distribution (Dehnen 1999, 2000) due to the rotation of the bar if the Sun is located at the bar's outer Lindblad resonance (OLR). Indeed, stars in the Galaxy will have their orbits elongated along or perpendicular to the major axis of the bar (orbits respectively called the LSR and OLR modes in the terminology of Dehnen 2000), depending upon their position relative to the resonances, and both types of orbits coexist at the OLR radius. Moreover, all orbits are regular in a 2-dimensional (2D) axisymmetric potential, but the perturbation of the triaxial bar will induce some chaos. Fux (2001) showed that in the region of the Hercules stream in velocity space, the chaotic regions, decoupled from the regular regions, are more heavily crowded. The Hercules stream has thus also been interpreted as an overdensity of chaotic orbits (Fux 2001) due to the rotating bar. Quillen (2003) has confirmed that when the effect of the spiral structure is added to that of the bar, the "chaotic" Hercules stream remains a strong feature of the local DF, whose boundaries are refined by the spiral structure. This stream in the local DF seems thus related to a non-axisymmetric perturbation rather than to a deviation from equilibrium due to inhomogeneous star formation. Following Mühlbauer & Dehnen (2003), the Galactic bar naturally induces a non-zero vertex deviation on the order of 10° and the vertex deviation found in Sects. 3.1 and 3.2 would thus be partly related to the Hercules stream. Nevertheless, the other streams present in the data are also partly responsible for the vertex deviation. The likely dynamical origin of the Hercules stream has been the first example of a non-axisymmetric origin for a stream in velocity space: the other streams could thus be related to other non-axisymmetric effects. Chereul & Grenon (2001) proposed that the Hyades supercluster represents in fact an extension of the Hercules stream, but the LM method has shown that the two features are clearly separated in the UV-plane.

De Simone et al. (2004) have shown that the structure of the local DF could be due to a lumpy potential related to the presence of transient spiral waves in the shearing sheet (i.e. a small portion of an infinitesimally thin disk that can be associated with the solar neighbourhood). Julian & Toomre (1966) have studied, in the shearing sheet, the response of a stellar disk to a point-like perturbation of the potential. They found that this response is in the form of density waves whose wavecrests swing around from leading to trailing. These waves are transient because their amplitudes are amplified transitorily and then die away. The duration of these transient spiral waves is of the order of an orbital period, i.e. of the order of 10^8 years, and they impart momentum to stars: this mechanism tends to put stars in some specific regions of the UV-plane in the simulations of De Simone et al. (2004), thus creating streams as observed in our sample. These spiral waves cause radial migration in the galactic disk near their corotation radius, while not increasing the random motions and preserving the overall angular momentum distribution (Sellwood & Binney 2002). The seemingly peculiar chemical composition of the group HyPl (i.e., a metallicity higher than average for field giants, as suggested by the 17 giant stars analyzed by McWilliam 1990 and displayed in Fig. 15, also reported by Chereul & Grenon 2001) thus suggests that the group has a common galactocentric origin in the inner Galaxy (where the interstellar medium is more metal-rich than in the solar neighbourhood) and that it was perturbed by a spiral wave at a certain moment. This specific scenario (Pont et al., in preparation) would explain why this group is composed of stars sharing a common metallicity but not a common age. The group Si could also be a clump recently formed by the passage of a transient spiral.

The simulations of De Simone et al. (2004) can create streams with a *range of 3 Gyr or more in age*, and this is thus a mechanism that can explain that main result of our study. Another characteristic of the simulations is that they tend to reproduce the observed branches, and their origin ultimately lies

in the same mechanism as that elucidated by Woolley (1961). However, the tilt of the branches in the UV-plane is not reproduced by the simulations.

A question which arises in the framework of this dynamical scenario is the following: is it by chance that such a large number of young clusters and associations are situated on the same branches in the UV-plane (more than half of the OB associations listed in Table A.1 of de Zeeuw 1999 are situated in the regions of the HyPl and Si groups in Fig. 9)? Probably not, which suggests that the same transient spiral which gave their peculiar velocity to the HyPl and Si groups has put these young clusters and associations along the same UV branches. For example, it is quite striking that the Hyades cluster itself is metal-rich with a mean [Fe/H] = 0.13 (Boesgaard 1989), thus pointing towards the same galactocentric origin as the HyPl group. The entire cluster could have been shifted in radius while remaining bound since the effect of a spiral wave on stars depends on the stars' phase with respect to the spiral, and the phase does not vary much across the cluster. Moreover, since most clusters and associations are young, they should not have crossed many transients, which suggests that the same spiral transient could have formed some clusters and associations (by boosting star formation in the gas cloud) and could at the same time have given them their peculiar velocity in the UV-plane. The relation between spiral waves and star formation is indeed well established (e.g. Hernandez et al. 2000 who found a star formation rate $SFR(t)$ with an oscillatory component of period 500 Myr related to the spiral pattern). As a corollary, we conclude that the dynamical streams observed among K and M giants are *young* kinematic features: integrating backwards (in a smooth stationnary axisymmetric potential) the orbits of the stars belonging to the streams makes thus absolutely no sense, and reconstructing the history of the local disk from the present data of stars in the solar neighbourhood becomes tricky. In this dynamical scenario, the deviation from dynamical equilibrium that is present among samples of young stars is closely related to the deviation from axisymmetry existing in the Galaxy. Of course, we do not exclude that the position of some clusters and OB associations in the same region of velocity space as the dynamical streams could be the result of chance (Chereul et al. 1998).

If this dynamical scenario is correct, the term "dynamical stream" for the branches in velocity space seems more appropriate than the term "supercluster" since they are not caused by contemporaneous star formation but rather involve stars that do not share a common place of birth: stars in the streams just share at present time a common velocity vector.

It should be noted that those non-axisymmetric perturbations, as well as the minor mergers, could lead to some asymmetries in the spatial distribution of stars in the galactic disk on a large scale (see Parker et al. 2004). Since our sample does not cover the whole sky, and is anyway restricted to the solar neighbourhood, we are not in a position to detect those asymmetries.

To conclude this section, let us stress that the dynamical, non-axisymmetric theory to explain the substructure observed in the velocity space is largely preferred over the theory that views it as remnants of clusters of stars sharing a common initial origin, essentially because of the wide range of ages of the stars composing the identified subgroups. In fact, we stress that the deviation from equilibrium among young stars (Dehnen & Binney 1998) and the dynamical streams exhibited in this paper could be closely related to each other. The presence of dynamical streams in our sample of K and M giants is clearly responsible for the vertex deviation found for late-type giants, but we even suggest that the same origin could hold as well for early-type stars. It is indeed quite striking on Fig. 9 that *the group Y extends just far enough in the UV-plane to touch both the HyPl and Si branches*. The presence of stars from these two streams in group Y (sent in that region of the UV-plane at the time of their formation because of the peculiar velocity imparted by the spiral wave that created them) imposes a very specific value to the vertex deviation (ranging from 15° to 30° and more), in agreement with the high values often observed for young stars (see Dehnen & Binney 1998). This idea that the vertex deviation for younger populations could in fact have the same *dynamical* origin as the vertex deviation for old ones was already proposed by Mayor (1972, 1974). Here, we also argue that even the specific initial conditions of young groups of stars could be due to the same phenomenon.

However, nature is of course not so simple and the features of the DF are presumably related to a mixture of several phenomena. Notably, the initial conditions in the simulations should be more complex than the simple 2D Schwarzschild velocity ellipsoid used by De Simone et al. (2004): in fact, purely *axisymmetric* substructure could already be present in the solar neighbourhood (see the structure of the UV-plane in Dejonghe & Van Caelenberg 1999). Other phenomena that could have an influence on the structure of velocity space are the following: a triaxial or clumpy dark halo, giant molecular clouds, and close encounters with the Magellanic Clouds (Rocha-Pinto et al. 2000). Theoretical investigations in this area should thus clearly be pursued.

4. Summary and perspectives

This paper presented the first kinematic analysis of 5311 K and 719 M giants (after excluding the binaries for which no center-of-mass velocity could be estimated) in the solar neighbourhood which included radial velocity data from an important survey performed with the CORAVEL spectrovelocimeter. We also used proper motions from the Tycho-2 catalogue.

First, we analyzed the kinematics of the sample restricted to the 2774 stars with parallaxes accurate to better than 20%, and then we made full use of the 6030 available stars and evaluated the kinematic parameters with a Monte-Carlo method. We found that the asymmetric drift is larger for M giants than for K giants due to the fact that the M giants must be a little older than the K giants on average. We also found the usual value for the solar motion when assuming that the whole sample has no net radial and vertical motion (Sect. 3.2).

Then a maximum-likelihood method, based on a Bayesian approach (Luri et al. 1996, LM method), has been applied to the data and allowed us to simultaneously derive maximum likelihood estimators of luminosity and kinematic parameters, and to identify subgroups present in the sample. Several subgroups can be identified with known kinematic features of the solar

neighbourhood (namely the Hyades-Pleiades supercluster, the Sirius moving group and the Hercules stream). Isochrones in the Hertzsprung-Russell diagram reveal a very wide range of ages for stars belonging to these subgroups. We thus conclude that this substructure in velocity space is probably related to the dynamical perturbation by transient spiral waves (as recently modelled by De Simone et al. 2004) rather than to cluster remnants. The emerging picture is thus one of dynamical streams pervading the solar neighbourhood. A possible explanation for the presence of young group/clusters in the same area of the UV-plane as those streams is that they have been put there by the spiral wave associated with their formation, while kinematics of the older stars of our sample have also been disturbed by the same wave. The seemingly peculiar chemical composition of the Hyades-Pleiades stream (also reported by Chereul & Grenon 2001) suggests that this stream originates from a specific galactocentric distance and that it was perturbed by a spiral wave at a certain moment and radially pushed by the wave in the solar neighbourhood (see Sellwood & Binney 2002; Pont et al., in preparation). This would explain why this stream is composed of stars sharing a common metallicity but not a common age. A careful metallicity analysis of this stream would be of great interest in order to confirm this scenario. The Sirius moving group could also be a feature recently formed by the passage of a transient spiral, while the Hercules stream would be related to the bar's outer Lindblad resonance (Dehnen 1999, 2000; Fux 2001). The position of all these streams in the UV-plane is responsible for the vertex deviation of $16.2^\circ \pm 5.6^\circ$ for the whole sample (see Sect. 3.2). We even argue that the vertex deviation observed among large samples of early-type stars (see Dehnen & Binney 1998) and the specific kinematic initial conditions of some young open clusters and OB associations could in fact have the same dynamical origin as those streams of giants. A better understanding of the streams should start with a chemical analysis of the stars belonging to them. As a first step, their photometric indices could be investigated. Note also that an important consequence of the dynamical origin of the streams is that it makes no sense to integrate backwards (in a smooth stationary axisymmetric potential) the orbits of the stars belonging to them.

The group of background stars (group B) has a distribution in velocity space close to a Schwarzschild ellipsoid but is not centered on the classical value found for $-U_\odot$ in Sect. 3.2 when considering the full sample, including the streams. Instead we find $\langle U \rangle = -2.78 \pm 1.07$ km s^{-1}. This discrepancy clearly raises the essential question of how to derive the solar motion in the presence of dynamical perturbations altering the kinematics of the solar neighbourhood (the net radial motion of stars in the solar neighbourhood can be of the order of 10 km s^{-1} in the simulation of De Simone et al. 2004): does there exist in the solar neighbourhood a subset of stars having no net radial motion which can be used as a reference against which to measure the solar motion?

Theoretical investigations in this area should thus clearly be pursued, and in particular *dynamical modeling*. We have shown that the fine structure of phase space in the solar neighbourhood cannot be interpreted in terms of an axisymmetric steady-state model. Nevertheless, an axisymmetric model revealing all the fine structure of the axisymmetric distribution function in the solar neighbourhood (Dejonghe & Van Caelenberg 1999; Famaey et al. 2002; Famaey & Dejonghe 2003) would give ideal initial conditions (more complex than a simple 2D Schwarzschild velocity ellipsoid; see especially the structure of the UV-plane in Dejonghe & Van Caelenberg 1999) for 3D N-body simulations that could afterwards reproduce some non-axisymmetric features observed in the solar neighbourhood (see Fux 1997; De Simone et al. 2004, for 2D simulations).

Acknowledgements. We thank R. Griffin for allowing us to derive the center-of-mass velocity of binaries from his unpublished CORAVEL data. Most of the existing orbits for K giants quoted in Table A.1 were derived by R. Griffin, and we want to recognize here his enormous and valuable contribution to this field. We also thank G. Traversa and B. Pernier for their important contribution to the observations with the CORAVEL spectrometer. This research was made possible by the substantial financial support received from the *Fonds National Suisse pour la Recherche scientifique* which funded the development of CORAVEL, and the operation of the Swiss 1-m telescope at the *Observatoire de Haute Provence.*

Appendix A: Contents of the data table

Table A.1[2] contains 6691 lines, and contains the following information in the successive columns (note that missing data are replaced by null values):

1 HIP number.
2 HD number.
3–4 BD number, only when there is no HD number.
5–6 Right ascension and declination in decimal degrees from fields H8 and H9 of the Hipparcos Catalogue (ICRS, equinox 2000.0; epoch 1991.25).
7–8 Hipparcos parallax and standard error.
9–10 $\mu_{\alpha*} \equiv \mu_\alpha \cos\delta$ from Tycho-2 and standard error.
11–12 μ_δ from Tycho-2 and standard error. For 291 stars, null values are found in Cols. 9 to 12; the kinematic study made then use of the Hipparcos proper motions instead of the Tycho-2 ones. In most cases, the absence of a Tycho-2 proper motion is caused by the fact that the star has a close visual companion or is too bright for the Tycho detection.
13–16 Same as Cols. 9 to 12 for Hipparcos proper motions.
17 The normalized absolute difference between the Hipparcos and Tycho-2 proper motions: $\Delta\mu = |\mu_{\rm Hip} - \mu_{\rm Tyc2}|/\epsilon_\mu$, where $\mu = (\mu_\alpha^2 \cos^2\delta + \mu_\delta^2)^{1/2}$ and $\epsilon_\mu = (\epsilon^2_{\mu_{\rm Hip}} + \epsilon^2_{\mu_{\rm Tyc-2}})^{1/2}$, where ϵ_i denotes the standard error of quantity i. The quantity $\Delta\mu$ may be used as a diagnostic tool to identify long-period binaries (Kaplan & Makarov 2003). The basic idea behind this tool is the following. For binary stars with orbital periods much longer than the duration of the Hipparcos mission, the proper motion recorded by Hipparcos is the vector addition of the true proper motion and of the orbital motion. This orbital motion averages out in the Tycho-2 value, since it is derived from measurements spanning a much

[2] Table A.1 is only available in electronic form at the CDS.

Table A.1. The left-hand side of the first page of Table A.1, fully available in electronic form at the CDS. See text for a description of the column contents.

HIP	HD	BD		α (°)	δ (°)	$\pi\pm$ (mas)		$\mu_{\alpha*,\mathrm{T-2}}\pm$ (mas)		$\mu_{\delta,\mathrm{T-2}}\pm$ (mas)		$\mu_{\alpha*,\mathrm{HIP}}\pm$ (mas)		$\mu_{\delta,\mathrm{HIP}}\pm$ (mas)		$\Delta\mu$
21	224724	0	0	0.06623569	8.00723437	5.84	0.95	62.5	1.2	−0.4	1.3	61.89	0.84	−0.22	0.56	−0.30
31	224760	0	0	0.09809390	2.67547768	1.84	1.05	−2.1	1.0	1.3	1.1	−4.88	1.49	−0.20	0.69	1.09
36	224759	0	0	0.10327550	12.26709303	6.30	0.96	49.5	1.1	15.6	1.1	49.71	0.85	14.27	0.60	−0.10
73	224826	0	0	0.22045719	66.84796687	3.97	0.69	−23.4	1.3	18.0	1.3	−20.78	0.67	18.19	0.55	−0.94
119	224894	0	0	0.39020229	44.67544581	7.49	0.83	−11.6	0.9	−17.0	1.0	−10.61	0.60	−18.37	0.51	0.41
121	224895	0	0	0.39647681	28.42377416	3.66	0.83	−18.7	1.1	−33.6	1.1	−18.88	0.66	−34.10	0.46	0.30
123	224891	0	0	0.40024110	72.23660619	5.07	0.70	−44.5	0.8	3.6	0.9	−44.73	0.57	3.74	0.53	0.17
136	224907	0	0	0.42864226	24.25318080	5.84	0.78	18.1	0.8	−29.0	0.8	18.50	0.71	−28.01	0.47	−0.44
142	224918	0	0	0.45374866	66.30600204	16.04	0.69	5.6	1.2	13.1	1.3	4.74	0.65	12.31	0.53	−0.54
181	224980	0	0	0.57381667	60.70319460	2.51	0.64	−7.9	1.2	−12.0	1.3	−8.91	0.50	−11.05	0.52	−0.09
258	225073	0	0	0.80532807	17.55239698	6.28	0.78	57.8	0.9	−52.8	0.9	58.45	0.74	−52.87	0.53	0.34
282	225106	0	0	0.87642718	19.38157170	1.62	0.97	−0.3	1.0	−29.4	1.0	0.04	0.77	−31.13	0.59	1.01
288	225105	0	0	0.88875927	42.35221969	5.49	0.97	99.1	1.1	−46.7	1.1	98.95	0.66	−46.75	0.61	−0.06
302	225136	0	0	0.96511407	66.71220273	3.31	0.60	9.9	1.0	−6.4	1.1	7.86	0.56	−8.15	0.46	−0.28
323	225172	0	0	1.04272795	49.87020726	6.15	0.89	−8.1	1.3	−11.8	1.3	−8.01	0.63	−10.94	0.60	−0.37
368	225221	0	0	1.15607578	2.93722463	4.83	1.03	18.7	1.1	0.9	1.1	20.68	1.07	1.42	0.81	0.98
374	225220	0	0	1.16704444	34.26519797	6.13	1.59	0.0	0.0	0.0	0.0	−15.80	1.51	−30.38	1.09	0.00
379	225216	0	0	1.17432297	67.16638761	10.30	0.58	95.1	1.2	24.7	1.3	95.58	0.48	23.80	0.45	0.13
399	225276	0	0	1.23302998	26.64879958	5.34	0.77	109.4	1.1	−13.1	1.1	112.32	0.71	−14.52	0.47	1.73
466	58	0	0	1.39547600	53.17169568	3.52	0.83	16.0	0.8	−0.4	0.8	16.36	0.67	−0.82	0.57	0.26
472	71	0	0	1.41549758	55.70990230	4.25	0.78	7.8	1.1	−1.8	1.2	8.82	0.63	−1.82	0.68	0.53
496	100	0	0	1.48628758	24.56904604	5.31	0.73	34.7	0.8	−16.8	0.8	34.93	0.61	−17.05	0.49	0.23
502	111	0	0	1.50224247	28.27696051	2.90	0.77	−7.0	1.1	−4.1	1.1	−5.09	0.63	−4.69	0.49	−0.68
504	112	0	0	1.51336417	24.91664125	5.66	0.82	82.7	1.1	−18.3	1.0	85.60	0.68	−16.84	0.52	1.48
525	145	0	0	1.58393383	40.89871965	8.60	0.73	83.3	1.0	8.2	1.1	82.91	0.74	10.65	0.58	−0.06
598	236	0	0	1.81025436	20.55571109	3.54	1.00	11.9	0.9	2.1	0.9	12.29	0.95	1.16	0.74	0.15
607	249	0	0	1.84365756	26.45088655	9.37	0.84	131.5	1.2	−119.4	1.2	131.20	0.83	−117.65	0.52	−0.71
625	279	0	0	1.90698995	40.07851976	5.37	0.80	35.9	1.4	−7.8	1.4	35.24	0.71	−8.78	0.55	−0.19
704	405	0	0	2.19110187	14.14205698	5.19	0.91	17.7	0.9	−33.5	0.9	18.87	0.75	−33.40	0.60	0.30
714	414	0	0	2.20832630	40.49456869	3.19	0.76	8.4	1.0	−6.4	1.1	7.09	0.73	−7.99	0.56	0.07
716	417	0	0	2.21695394	25.46285169	7.78	0.81	103.5	1.1	55.1	1.0	104.61	0.83	54.77	0.51	0.47
755	443	0	0	2.31906353	65.07079864	17.03	0.69	130.9	1.3	37.0	1.4	128.28	0.69	38.30	0.62	−1.01
779	0	61	8	2.40151993	62.66781255	4.76	2.01	0.0	0.0	0.0	0.0	−2.50	1.80	2.02	2.03	0.00
799	529	0	0	2.46856966	12.71084240	5.18	1.15	−6.3	1.3	−6.0	1.2	−6.09	0.98	−5.73	0.68	−0.16
824	559	0	0	2.52286733	25.19788575	3.13	0.90	4.3	0.9	10.6	0.9	4.16	0.81	9.10	0.58	−0.89
834	553	0	0	2.54377402	64.64672491	4.74	0.83	−29.2	1.3	−4.1	1.4	−30.17	0.84	−4.08	0.76	0.43
852	598	0	0	2.61150772	28.65292193	3.65	0.87	−6.6	1.2	−16.0	1.1	−5.04	0.81	−16.73	0.54	0.09
858	613	0	0	2.63506952	33.13088570	4.74	0.76	−24.7	1.2	−0.6	1.2	−25.63	0.75	−0.52	0.51	0.48
868	632	0	0	2.66362432	2.30067277	2.91	0.97	0.1	1.0	1.9	1.1	0.04	0.94	3.36	0.67	0.77
871	232121	0	0	2.67528589	54.89149475	1.74	2.12	0.0	0.0	0.0	0.0	−1.90	1.87	−0.81	1.82	0.00
902	663	0	0	2.78289623	57.58791462	4.43	0.73	−37.3	1.0	11.3	1.1	−37.27	0.53	11.00	0.55	−0.07
909	685	0	0	2.81532971	7.94816079	4.21	1.02	−10.8	0.8	−8.3	0.9	−10.76	0.85	−6.87	0.65	−0.53
918	678	0	0	2.84178323	74.48458019	6.06	0.67	73.3	0.9	−13.3	1.1	73.95	0.65	−15.28	0.53	0.62
967	743	0	0	2.99596734	48.15237121	5.93	0.70	59.5	1.5	10.8	1.5	60.54	0.46	10.39	0.45	0.43
969	756	0	0	3.00550041	23.47174032	6.88	0.76	87.1	0.9	3.8	0.9	86.82	0.66	3.73	0.46	−0.19
972	754	0	0	3.00807432	48.68005386	3.49	1.01	17.5	1.5	32.4	1.5	18.32	0.78	33.73	0.69	0.66
980	763	0	0	3.02849022	47.49116017	6.68	0.87	−13.7	0.9	−25.3	1.1	−13.46	0.65	−24.35	0.56	−0.57
982	762	0	0	3.03640453	48.18225854	3.46	0.87	17.9	1.1	−4.5	1.2	16.16	0.60	−2.94	0.56	−1.11
989	784	0	0	3.06609863	22.55671394	2.89	0.85	19.8	0.7	9.4	0.7	19.02	0.82	8.66	0.53	−0.73

Table A.1. continued.

HIP	Hp ±		V_{T2}	Hp − V_{T2}	$V-I$ H40	$V-I$ new	B	v_r ± (km/s)		$M_{H\mathrm{p}}$	d ± (pc)		A_V	U	V (km/s)	W	g	P(g) (%)	R.
21	7.6923	0.0012	7.683	0.009	1.43	1.24	*	−11.72	0.16	1.29	184.4	28.0	0.07	−42.5	−31.4	−1.6	3	49.7	
31	7.7648	0.0020	7.793	−0.028	1.46	1.47	*	3.52	0.21	−0.67	471.6	131.2	0.07	6.5	6.2	−0.6	5	61.6	
36	7.8503	0.0015	7.805	0.045	1.11	1.00	0	0.00	0.00	0.00	0.0	0.0	0.00	0.0	0.0	0.0	0	0.	
73	7.0364	0.0011	7.054	−0.018	1.44	1.41	*	−11.91	0.20	−0.51	245.6	35.3	0.60	24.9	−1.6	24.9	3	90.4	
119	6.9834	0.0010	6.934	0.049	1.04	0.97	*	0.53	0.21	0.95	146.4	18.1	0.20	10.3	1.9	−9.6	5	58.7	
121	6.9957	0.0011	6.964	0.032	1.16	1.09	*	−15.96	0.21	−0.33	272.1	48.0	0.15	43.0	−20.2	−21.9	3	97.7	
123	7.3790	0.0013	7.342	0.037	1.13	1.05	*	−13.32	0.22	0.36	203.0	26.3	0.49	42.0	7.3	9.3	3	90.6	
136	6.7635	0.0010	6.722	0.041	1.12	1.02	*	−7.69	0.21	0.31	182.6	25.0	0.15	−5.6	−24.8	−17.7	3	77.9	
142	7.4726	0.0013	7.404	0.069	0.78	0.83	*	−21.68	0.24	3.29	63.7	2.9	0.16	6.9	−20.4	2.1	3	68.3	
181	6.7960	0.0034	6.980	−0.184	2.46	2.30	*	−21.39	0.23	−1.98	377.9	67.0	0.89	25.8	−11.4	−17.8	1	54.4	
258	6.7616	0.0008	6.713	0.049	1.08	0.97	*	−18.50	0.21	0.56	162.5	16.3	0.15	−17.5	−56.3	−23.8	6	71.4	
282	8.0651	0.0018	8.075	−0.010	1.39	1.36	*	−47.28	0.22	−0.73	535.3	144.5	0.15	47.3	−73.3	−21.8	2	44.8	
288	8.0688	0.0013	8.028	0.041	1.04	1.03	*	3.33	0.38	1.36	197.5	32.8	0.23	−70.3	−49.2	−58.6	2	49.9	
302	6.3544	0.0045	6.520	−0.166	2.28	2.22	0	0.00	0.00	0.00	0.0	0.0	0.00	0.0	0.0	0.0	0	0.	
323	7.5413	0.0010	7.475	0.066	0.98	0.85	*	−16.05	0.39	0.92	192.9	34.6	0.19	11.5	−11.8	−5.6	3	76.8	
368	8.0579	0.0016	8.045	0.013	1.21	1.21	*	−16.06	0.22	0.83	270.3	67.3	0.07	−19.9	−18.6	9.9	3	52.0	
374	7.1831	0.0011	7.255	−0.072	0.96	1.73	4	−23.98	0.29	0.27	216.8	56.2	0.23	29.3	−22.9	−13.0	3	97.4	
379	5.8511	0.0006	5.794	0.057	1.02	0.92	*	−28.43	0.20	0.61	99.5	5.7	0.25	−27.1	−47.2	1.0	6	64.3	
399	6.3941	0.0010	6.415	−0.021	1.34	1.43	0	0.00	0.00	0.00	0.0	0.0	0.00	0.0	0.0	0.0	0	0.	
466	7.3999	0.0009	7.358	0.042	1.14	1.02	*	−9.72	0.22	−0.39	314.7	51.6	0.30	−14.6	−20.3	−3.3	4	46.2	
472	7.1505	0.0009	7.115	0.035	1.15	1.06	0	0.00	0.00	0.00	0.0	0.0	0.00	0.0	0.0	0.0	0	0.	
496	7.0181	0.0012	7.067	−0.049	1.58	1.60	*	−14.36	0.22	0.37	199.1	27.1	0.15	−18.3	−32.9	−9.4	3	57.3	
502	6.7361	0.0007	6.774	−0.038	1.58	1.53	*	9.98	0.20	−1.14	350.5	77.3	0.15	5.7	9.9	−9.0	5	59.9	
504	7.6749	0.0012	7.608	0.067	1.07	0.85	*	−10.40	0.21	1.15	188.2	20.7	0.15	−54.5	−49.0	−19.4	6	82.7	
525	7.0996	0.0008	7.062	0.038	1.05	1.05	*	−73.82	0.25	1.49	121.7	11.1	0.18	−14.1	−83.7	22.6	2	94.9	
598	8.1267	0.0015	8.126	0.001	1.44	1.29	*	29.49	0.23	0.09	378.5	109.4	0.15	−20.4	12.5	−20.3	3	92.4	
607	7.4919	0.0011	7.438	0.054	0.99	0.94	*	16.44	0.22	2.14	110.4	10.0	0.14	−41.5	−47.7	−71.0	2	90.8	
625	7.5541	0.0008	7.503	0.051	0.98	0.96	*	−15.02	0.51	0.96	188.0	20.8	0.23	−16.3	−29.0	−6.1	4	49.3	
704	8.0043	0.0013	7.947	0.057	1.09	0.91	*	−37.60	0.22	1.05	237.8	38.2	0.07	11.2	−56.0	−0.4	6	46.4	
714	6.9335	0.0012	6.990	−0.056	1.59	1.64	*	−11.78	0.54	−1.14	370.0	82.0	0.24	3.8	−19.4	−8.3	1	57.5	
716	6.4099	0.0006	6.354	0.056	0.97	0.92	*	16.11	0.20	0.71	129.3	12.6	0.15	−72.5	−1.4	6.6	3	92.4	
755	7.1836	0.0010	7.128	0.056	0.93	0.93	*	5.00	0.22	3.15	59.7	2.4	0.15	−37.0	−14.0	4.5	3	63.9	
779	9.4783	0.0041	9.750	−0.272	2.22	2.68	9	−74.31	0.13	−5.78	3601.3	771.2	2.47	158.0	−51.3	40.7	1	59.2	*
799	8.5304	0.0016	8.471	0.059	1.04	0.90	*	−1.34	0.53	1.03	306.6	100.3	0.07	11.2	−2.1	−3.1	3	51.6	
824	7.8382	0.0022	7.985	−0.147	2.15	2.13	*	18.91	0.22	−0.08	357.1	87.1	0.15	−13.7	19.4	1.6	3	86.5	
834	8.2793	0.0043	8.263	0.016	1.00	1.19	1	−38.93	0.30	0.67	251.4	47.7	0.61	46.7	−17.2	−0.7	3	98.2	*
852	7.0964	0.0048	7.345	−0.249	2.64	2.59	*	−14.17	0.34	−0.53	312.1	72.7	0.15	19.4	−16.4	−10.1	3	86.2	
858	6.9629	0.0007	6.970	−0.007	1.42	1.34	*	−15.05	0.26	−0.05	226.9	37.5	0.24	28.8	0.5	10.9	3	64.2	
868	8.3296	0.0013	8.298	0.032	1.13	1.09	*	−40.89	0.23	0.10	428.5	126.7	0.07	9.0	−18.4	36.9	3	80.2	
871	9.1126	0.0393	9.133	−0.020	0.73	1.42	6	−6.50	0.30	−1.39	934.2	319.8	0.65	17.1	−1.4	−1.3	1	38.0	*
902	6.8469	0.0010	6.821	0.026	1.17	1.13	*	−16.90	0.31	−0.42	221.4	30.7	0.54	40.6	3.4	19.2	3	89.8	
909	7.8542	0.0016	7.806	0.048	1.12	0.98	*	−24.72	0.22	0.29	315.9	89.6	0.07	17.8	−14.4	15.3	3	97.3	
918	7.3180	0.0012	7.264	0.054	0.98	0.94	*	0.32	0.21	1.05	169.9	18.0	0.12	−53.6	−24.9	−19.4	3	61.1	
967	6.3113	0.0009	6.336	−0.025	1.48	1.45	*	14.25	0.20	−0.07	174.1	20.1	0.17	−51.0	−9.4	−2.4	3	74.4	
969	6.7432	0.0006	6.688	0.055	0.97	0.93	*	8.57	0.21	0.73	148.5	15.6	0.15	−54.1	−21.2	−12.6	3	56.8	
972	8.3410	0.0017	8.297	0.044	1.02	1.01	0	0.00	0.00	0.00	0.0	0.0	0.00	0.0	0.0	0.0	0	0.	
980	7.5299	0.0011	7.484	0.046	1.04	0.99	*	4.36	0.14	1.31	162.6	21.6	0.16	12.7	5.4	−18.1	5	51.5	
982	7.7598	0.0015	7.758	0.002	1.28	1.28	*	−19.64	0.21	−0.17	333.4	75.6	0.31	−14.4	−31.5	−6.3	3	48.1	
989	7.7254	0.0065	7.919	−0.194	2.39	2.35	*	−10.26	0.59	−0.17	354.7	77.7	0.15	−33.9	−15.0	13.4	3	71.4	

Notes:
779 Very distant star (first-order correction to the differential galactic rotation inaccurate); binary of VV Cep type (M1epIb + B2.6V).
834 2002A&A...395..885D.
871 12.154,1988A&A...207...37A.

longer time base (of the order of a century, as compared to 3 yr for Hipparcos). Therefore, a difference between the Tycho-2 and Hipparcos proper motions (beyond the combined error bar encapsulated by ϵ_μ) very likely hints at the binary nature of the star. This diagnostic will be fully exploited in a forthcoming paper devoted to the binary stars present in our sample. Note that Fig. 1 presents the histogram of $\Delta\mu$, which indeed reveals the presence of an abnormally large tail at $\Delta\mu \geq 1.5$.

18–19 Hipparcos H_p magnitude and associated standard error.

20 Tycho-2 V_{T2} magnitude.

21 $H_p - V_{T2}$. For visual binaries (flag 4 in Col. 24), this colour index has not been listed and the value 0.0 is given instead, because the H_p magnitude appears to be a composite value for the two visual components. In most of these cases, the V_{T2} magnitude of the visual companion is given in the last column of the table. For large amplitude variable stars, the $H_p - V_{T2}$ index is meaningless as well, and as been set to 0.

22 $V - I$ colour index in Cousins' system as provided by field H40 of the Hipparcos catalogue. This index is useful for constructing the Hertzsprung-Russell (HR) diagram of the sample. It should be stressed that the H40 field of the Hipparcos catalogue does not provide a directly measured quantity. It has instead been computed from various colour transformations based on the $B - V$ index from field H37, which neither is a directly measured quantity.

23 $V-I$ colour index in Cousins' system as provided by the colour transformation based on the *measured* $H_p - V_{T2}$ colour index (Platais et al. 2003). This value is thus in principle more reliable than the Hipparcos H40 value (note, however, that the colour transformation provided by Platais et al. (2003) had to be extrapolated somewhat, since it is provided in the range $-2.5 \leq H_p - V_{T2} \leq -0.20$, whereas our data set goes up to $H_p - V_{T2} = 0.1$). It has been used to draw the HR diagram of the sample. For large-amplitude variable stars, the median $V - I$ index has been taken directly from Platais et al. (2003), instead of being computed from the colour transformation based on $H_p - V_{T2}$ (set to 0. in those cases).

24 Binarity flag:
*: no evidence for radial-velocity variations;
0: spectroscopic binary (SB), with no orbit available. The star had to be discarded from the kinematic analysis;
1: SB with an orbit available, or with a center-of-mass velocity which can be estimated reasonably well. Column 25 then contains the system's center-of-mass velocity. The reference with the orbit used to derive the center-of-mass velocity is listed in the last column. If no reference is given, the center-of-mass velocity has been estimated from the available CORAVEL data;
2: supergiant star, with a substantial radial-velocity jitter (see Fig. 5);
3: uncertain case: either SB or supergiant;
4: visual binary with a companion less than 6″ away (as listed by the Tycho-2 catalogue);
5, 6, 7, 8: as 0, 1, 2, 3 but for a visual binary. It should be stressed here that visual binaries have not been searched for exhaustively among our target stars. Whenever the Tycho-2 catalogue lists a companion star less than 6″ away from the target star, the binarity flag has been set to 4. In most of these cases, the Hipparcos H_p magnitude corresponds to the composite magnitude and the Tycho-2 proper motions are identical for the two components. The V_{T2} magnitude of the companion is listed in the last column of the table;
9: binary supergiant with an orbit available.

25–26 Average radial velocity (based on CORAVEL observations) or center-of-mass velocity for SBs (the last column provides the bibliographic code of the reference providing the orbit used), and standard error (set to 0.3 km s^{-1} in the case of center-of-mass velocity).

27 The absolute H_p magnitude, corrected for interstellar reddening (according to the model of Arenou et al. 1992), and based on the LM distance listed in Col. 28.

28–29 The maximum-likelihood distance based on the LM estimator (see Sect. 3.3), and its associated standard error (see Eq. (32)).

30 The interstellar absorption A_V, based on the LM distance and the model of Arenou et al. (1992).

31–33 The U, V and W components of the heliocentric space velocity deduced from the LM method (corrected for the galactic differential rotation to first order using $A = 14.82\,\mathrm{km\,s^{-1}\,kpc^{-1}}$ and $B = -12.37\,\mathrm{km\,s^{-1}\,kpc^{-1}}$).

34–35 The most likely group to which the star belongs, and the associated probability. The various groups are the following:
1 or Y: stars with a young kinematics;
2 or HV: high-velocity stars;
3 or B: stars defining the smooth background (the most populated group);
4 or HyPl: stars belonging to the Hyades-Pleiades stream;
5 or Si: stars belonging to the Sirius stream;
6 or He: stars belonging to the Hercules stream.

36 In the case of a spectroscopic binary with an available orbit: bibliographic code (according to the standard ADS/CDS coding) of the reference listing the orbit used as the source of the center-of-mass velocity (The code 2005A&A..J refers to the forthcoming paper by Jorissen et al. 2005 devoted to the analysis of the binary content of the present sample). In the case of a visual binary, the V_{T2} magnitude of the companion. An asterisk in that column indicates the presence of a note in the remark file.

It must be stressed that Cols. 27 to 35 contain model-dependent data, as they were derived by the LM method. They depend upon, e.g., the particular choice for the values of the Oort constants, the interstellar extinction model, the a priori choice of the various distribution functions.

References

Alvarez, R., Jorissen, A., Plez, B., et al. 2001, A&A, 379, 305
Arenou, F., Grenon, M., & Gómez, A. E. 1992, A&A, 258, 104
Baranne, A., Mayor, M., & Poncet, J. L. 1979, Vistas Astron., 23, 279
Baranne, A., Queloz, D., Mayor, M., et al. 1996, A&AS, 119, 373
Benz, W., & Mayor, M. 1981, A&A, 93, 235
Bienaymé, O. 1999, A&A, 341, 86
Blaauw, A. 1970, in The spiral structure of our galaxy, ed. W. Becker, & G. Contopoulos (Dordrecht), IAU Symp., 38, 199
Boesgaard, A. M. 1989, ApJ, 336, 798
Boutloukos, S., & Lamers, H. 2003, MNRAS, 338, 717
Bullock, J. S., & Johnston, K. V. 2004, in Satellites and Tidal Streams, ed. F. Prada, D. Martinez-Delgado, & T. Mahoney, in press [arXiv:astro-ph/0401625]
Brosche, P., Schwan, H., & Schwarz, O. 2001, Astron. Nachrichten, 322, 15
Brown, A. G. A., Arenou, F., van Leeuwen, F., Lindegren, L., & Luri, X. 1997, in The Hipparcos Venice Symp., ed. M. A. C. Perryman, ESA SP-402, 63
Chereul, E., Crézé, M., & Bienaymé, O. 1998, A&A, 340, 384
Chereul, E., Crézé, M., & Bienaymé, O. 1999, A&A, S135, 5
Chereul, E., & Grenon, M. 2001, in Dynamics of star clusters and the Milky Way, ed. S. Deiters, B. Fuchs, A. Just, R. Spurzem, & R. Wielen, ASP Conf., 228, 398
de Bruijne, J. H. J., Hoogewerf, R., Brown, A. G. A., et al. 1997, in The Hipparcos Venice Symp., ed. M. A. C. Perryman, ESA SP-402, 575
Dehnen, W. 1998, AJ, 115, 2384
Dehnen, W. 1999, ApJ, 524, L35
Dehnen, W. 2000, AJ, 119, 800
Dehnen, W., & Binney, J. J. 1998, MNRAS, 298, 387
Dejonghe, H., & Van Caelenberg, K. 1999, in AGB stars, ed. T. Le Bertre, A. Lèbre, & C. Waelkens, IAU Symp., 191 (ASP), 501
De Simone, R. S., Wu, X., & Tremaine, S. 2004, MNRAS, 350, 627
de Zeeuw, P. T., Hoogerwerf, R., de Bruijne, J. H. J., Brown, A. G. A., & Blaauw, A. 1999, AJ, 117, 354
Eggen, O. J. 1958, MNRAS, 118, 65
Eggen, O. J. 1960, MNRAS, 120, 563
Eggen, O. J. 1975, PASP, 87, 37
Eggen, O. J. 1983, MNRAS, 204, 377
Eggen, O. J. 1994, in Galactic and Solar System Optical Astrometry, ed. L. Morrison, & G. Gilmore (Cambridge: Cambridge University Press), 191
ESA 1997, The Hipparcos Catalogue, ESA SP-1200
Famaey, B., Van Caelenberg, K., & Dejonghe, H. 2002, MNRAS, 335, 201
Famaey, B., & Dejonghe, H. 2003, MNRAS, 340, 752
Feast, M., & Whitelock, P. 1997, MNRAS, 291, 683
Figueras, F., Gomez, A. E., Asiain, R., et al. 1997, in The Hipparcos Venice Symp., ed. M. A. C. Perryman, ESA SP-402, 519
Fux, R. 1997, A&A, 327, 983
Fux, R. 2001, A&A, 373, 511
Girardi, L., & Salaris, M. 2001, MNRAS, 323, 109
Helmi, A., White, S. D. M., de Zeeuw, P. T., & Zhao, H. 1999, Nature, 402, 53
Hernandez, X., Valls-Gabaud, D., & Gilmore, G. 2000, MNRAS, 316, 605
Høg, E., Fabricius, C., Makarov, V. V., et al. 2000, A&A, 355, L27
Ibata, R., Gilmore, G., & Irwin, M. 1994, Nature, 370, 194
Jorissen, A., & Mayor, M. 1988, A&A, 198, 187
Jorissen, A., Famaey, B., Dedecker, M., et al. 2004, Rev. Mex. Astron. Astrophys., Serie Conf., 21, 71
Julian, W. H., & Toomre, A. 1966, ApJ, 146, 810
Kaplan, G. H., & Makarov, V. V. 2003, Astron. Nachrichten, 324, 419
Kendall Sir, M., & Stuart, A. 1979, The advanced theory of statistics, Charles Griffin & Co. Ltd, Vol. II, 38
Kovalevsky, J. 1998, ARA&A, 36, 99
Lejeune, T., & Schaerer, D. 2001, A&A, 366, 538
Lindblad, B. 1925, Ark. Mat. Astron., 19A, 21
Luri, X. 1995, Ph.D. Thesis, Universitat de Barcelona
Luri, X., Mennessier, M. O., Torra, J., & Figueras, F. 1996, A&AS, 117, 405
Luri, X., & Arenou, F. 1997, in The Hipparcos Venice Symp., ed. M. A. C. Perryman, ESA SP-402, 449
Malmquist, K. G. 1936, Stockholms Ob. Medd., No 26
Mayor, M. 1972, A&A, 18, 97
Mayor, M. 1974, A&A, 32, 321
McWilliam, A. 1990, ApJS, 74, 1075
Montes, D., Lopez-Santiago, J., Galvez, M. C., et al. 2001, MNRAS, 328, 45
Mühlbauer, G., & Dehnen, W. 2003, A&A, 401, 975
Navarro, J. F., Helmi, A., & Freeman, K. C. 2004, ApJ, 601, L43
Nordström, B., Mayor, M., Andersen, J., et al. 2004, A&A, 418, 989
Oort, J. H. 1927, Bull. Astron. Inst. Neth., 4, 79
Parker, J. E., Humphreys, R. M., & Beers, T. C. 2004, AJ, 127, 1567
Platais, I., Pourbaix, D., Jorissen, A., et al. 2003, A&A, 397, 997
Quillen, A. C. 2003, AJ, 125, 785
Raboud, D., Grenon, M., Martinet, L., Fux, R., & Udry, S. 1998, A&A, 335, L61
Rocha-Pinto, H. J., Scalo, J., Maciel, W. J., & Flynn, C. 2000, A&A, 358, 869
Schwarzschild, K. 1907, Göttingen Nachr., 1907, 614
Sellwood, J. A., & Binney, J. J. 2002, MNRAS, 336, 785
Skuljan, J., Hearnshaw, J. B., & Cottrell, P. L. 1999, MNRAS, 308, 731
Soubiran, C., Gómez, A. E., Arenou, F., & Bougeard, M. L. 1990, in Errors, Bias and Uncertainities in Astronomy, ed. C. Jaschek, & F. Murtagh (Cambridge University Press), 407
Soubiran, C., Bienaymé, O., & Siebert, A. 2003, A&A, 398, 141
Trumpler, R. J., & Weaver, H. F. 1953, Statistical Astronomy (Berkeley: University of California Press)
Udry, S., Mayor, M., Andersen, J., et al. 1997, in The Hipparcos Venice Symp., ed. M. A. C. Perryman, ESA SP-402, 693
Van Eck, S., & Jorissen, A. 2000, A&A, 360, 196
Weidemann, V., Jordan, S., Iben, I., & Casertano, S. 1992, AJ, 104, 1876
Woolley, R. 1961, The Observatory, 81, 203
Zhu, Z. 2000, PASJ, 52, 1133